PLOS COMPUTATIONAL BIOLOGY

RESEARCH ARTICLE

Stochastic model of IP_3-induced Ca^{2+} spiking of HEK293 cells

Caterina Azzoni[1,2*], **Rene Jüttner**[1], **Anje Sporbert**[1], **Michael Gotthardt**[1,3,4], **H. Llewelyn Roderick**[5], **Martin Falcke**[1,6*]

1 Max Delbrück Center for Molecular Medicine (MDC), Berlin, Germany, **2** Faculty of Life Sciences, Humboldt-Universität zu Berlin, Berlin, Germany, **3** DZHK (German Centre for Cardiovascular Research), Partner Site Berlin, Berlin, Germany, **4** Charité-Universitätsmedizin, Berlin, Germany, **5** Department of Cardiovascular Sciences, Experimental Cardiology, KU Leuven, Belgium, **6** Department of Physics, Humboldt-Universität zu Berlin, Berlin, Germany

* caterina.azzoni@mdc-berlin.de (CA); martin.falcke@mdc-berlin.de (MF)

Citation: Azzoni C, Jüttner R, Sporbert A, Gotthardt M, Llewelyn Roderick H, Falcke M (2025) Stochastic model of IP_3-induced Ca^{2+} spiking of HEK293 cells. PLoS Comput Biol 21(8): e1013322. https://doi.org/10.1371/journal.pcbi.1013322

Editor: Philipp Martin Altrock, University of Kiel Faculty of Medicine: Christian-Albrechts-Universitat zu Kiel Medizinische Fakultat, GERMANY

Received: February 3, 2025

Accepted: July 10, 2025

Published: August 22, 2025

Data availability statement: Fluorescence intensity time-series data are available at Zenodo: https://doi.org/10.5281/zenodo.15705673. Analysed calcium spike trains are available at Zenodo: https://doi.org/10.5281/zenodo.14779474. Analysis scripts are available on GitHub: https://github.com/azzonic/calcium_spiketrains_analysis.

Abstract

Mathematical theory that accounts for the stochastic character of spike sequences of IP_3-induced Ca^{2+} signalling calculates the probability distributions of the features of the $[Ca^{2+}]_i$ time course, their moments and correlations. Including slow feedback from $[Ca^{2+}]_i$ to components of the pathway poses a challenge to stochastic modelling. Here, we present a stochastic model that takes this feedback into account, allows for a non-linear dependency of the open probability of the Inositol 1,4,5-trisphosphate receptor channel (IP_3R) on the feedback variable and the inclusion of more than one feedback with different relaxation time scales. We use this novel modelling approach to describe the effect of ER depletion by non-linear rate expressions for Ca^{2+}-induced Ca^{2+} release (CICR) and the measured non-linear IP_3-dependency of the open probability as part of the dynamic feedback. Our theory can calculate spike amplitude distributions, correlation coefficients (C_c) of interspike intervals (ISIs) and amplitudes, simulate ISI distributions and calculate their moments. We apply it to experiments with HEK293 cells. We find very good agreement between theoretical ISI distributions and their moments with experimental results. Many measured C_cs show positive values in accordance with the ideas formulated by our theory. Surprisingly, most ISI-amplitude correlations are weak despite the decay of negative feedback during the ISI, which affects spike probability. We even find negative values of C_cs, which indicate feedback that decreases the open probability of IP_3R with increasing ISI. The components of the pathway causing this anticorrelation have not yet been identified. Our data suggest that they involve components that are subject to cell variability.

Author summary

Ca^{2+} is a versatile second messenger. Ca^{2+} signals show stochastic spike timing and large cell variability despite their signal transmission function. Spike train properties, which are not subject to cell variability and thus define the system, are related to noise.

Funding: The author(s) received no specific funding for this work.

Competing interests: The authors have declared that no competing interests exist.

Hence, the first step in theoretical comprehension must be a stochastic theory. This study reports on progress in developing that theory and on experimental results. The application to Ca^{2+} signals in HEK293 cells meets basic expectations and, in part, explains the surprising results on ISI-amplitude correlations. The measured anticorrelation requires us to expand our ideas on feedback during spiking and the corresponding stochastic theory. Once we understand the role of fluctuations, we may also derive deterministic approximations for simulating averages.

Introduction

IP_3-induced Ca^{2+} signalling transmits information that arrives in the form of an agonist concentration at the cell plasma membrane to intracellular targets through changes in cytosolic $[Ca^{2+}]_i$ [6–11]. We introduce the pathway and some terms and definitions in Fig 1. Intracellular Ca^{2+} signals may be local/subcellular (puffs), sequences of $[Ca^{2+}]_i$ spikes (see Fig 1), or a long-lasting increase in $[Ca^{2+}]_i$ (overstimulation) [8,12]. The variability of the Ca^{2+} signals and of the average interspike interval (T_{av}) among cells stimulated with the same concentration of agonist is large [9,13]. Furthermore, the interpuff interval (IPI) and the interspike interval (ISI) are random [9,13,14]. This randomness and variability in the response to an identical stimulation (identical initial signal) in an information-transmitting system raises several basic questions, most notably how such a system can transmit information at all.

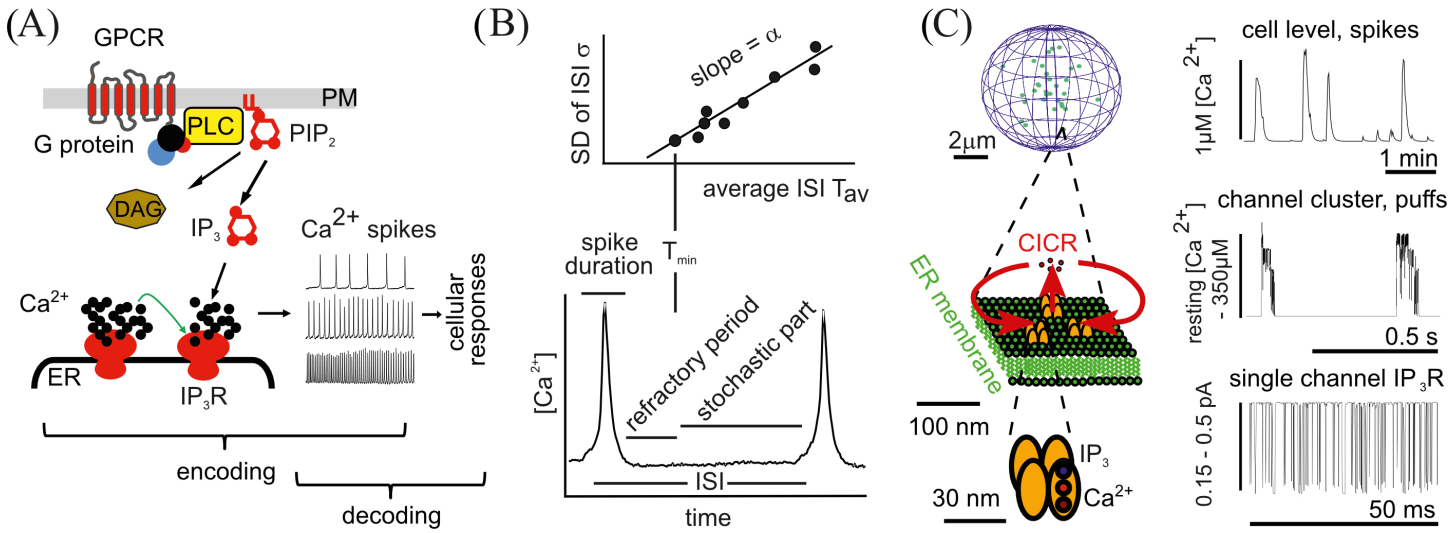

Fig 1. (A) Inositol 1,4,5-trisphosphate (IP_3) pathway of Ca^{2+} signaling. Binding of an agonist to one of a large family of G-protein coupled receptors (GPCR) activates phospholipase C (PLC), which produces IP_3 from phosphatidylinositol-4,5-bisphosphate (PIP_2). IP_3 sensitises IP_3 receptor channels (IP_3R) in the endoplasmic reticulum (ER) membrane to binding of Ca^{2+}, such that Ca^{2+} released from the ER through open channels increases the open probability of closed channels by Ca^{2+}-induced Ca^{2+}-release (CICR). PLC activates additional feedback to the IP_3R open probability via diacylglycerol (DAG). (B) The interspike interval (ISI) comprises the spike duration, the refractory period, and the stochastic part t_{sto}. The sum of spike duration and refractory period is T_{min}. It is a parameter of the theory and constant throughout a spike train. The sum of T_{min} and a realisation of t_{sto} ($T_{min} + t_{sto}$) is a realisation of an ISI. The average ISI is denoted T_{av} and the average of t_{sto} is T_{sto}. $T_{av}=T_{min}+T_{sto}$ holds. T_{av} and the standard deviation (SD) of ISI σ are linearly related with slope α. (C) IP_3-induced Ca^{2+} signalling is hierarchical with channels (comprising a tetramer of IP_3R proteins) on the lowest structural level, channel clusters as intermediate structure and cluster arrays on the cell level. Each structural level has its typical time scale and signal (see [1–5] for local currents and concentrations). The state of the IP_3R is determined by IP_3 and Ca^{2+} binding to the IP_3R tetramer. Channel clusters are the elementary units of cellular dynamics. Their release events are Ca^{2+} puffs generated by CICR. CICR entails excitability. Clusters cooperate by CICR in generating cellular Ca^{2+} spikes as global events. This study considers the dynamics of spike generation by clusters under global feedback that acts on all clusters.

https://doi.org/10.1371/journal.pcbi.1013322.g001

This question has found a partial answer: The average frequency of a spike sequence is the inverse of the average ISI. Agonist concentration steps induce changes in the average of the stochastic part of ISI in all cells by the same factor [9]. This can be likened to a melody which is a sequence of sound frequency ratios. Since a sequence of agonist concentration steps elicits the same sequence of frequency ratios in all cells, all cells play the same melody. However, due to the large variability of the average ISI between cells, each cell plays at its own pitch [9]. We still do not know how the cell-to-cell variability of the pitch can be reconciled with the signal transmission function of the system.

Concerning biophysical modelling, the conceptual questions to be addressed are: 1) what should be modelled given the lack of a unique response, 2) how can models be parameterised given variability and randomness, 3) which general rules can models reveal despite variability and randomness. The cumulant relation between the standard deviation (SD) of ISI and the average ISI introduced one general rule, which states that its slope α is conserved within cell variability and is specific to a cell type and agonist [9,13,15–17]. The concentration-response relationship of the average ISI (mentioned above) revealed that the average ISI depends exponentially on the concentration of the agonist. The agonist sensitivity γ is the same for all individual cells stimulated with the same agonist. Cell variability affects only the exponential prefactor [9]. Both conserved properties relate to stochastic aspects of Ca^{2+} spiking. Although obvious for α, it also applies to γ, as stimulation controls the stochastic part of the ISI [9]. Several theoretical studies on stochastic aspects of Ca^{2+} signalling have been published to address the questions related to this system [17–31]. Here, we report progress in developing a theory that focuses on the calculation of ISI and amplitude statistics.

The $[Ca^{2+}]_i$ signal can be induced either by Ca^{2+} entry from the extracellular space through plasma membrane channels, or by Ca^{2+} release from intracellular storage compartments, primarily located in the endoplasmic reticulum (ER). In the following, we will focus on IP_3-induced Ca^{2+} release from ER, which is the predominant Ca^{2+} release mechanism in many cell types (see Fig 1) [32].

The released Ca^{2+} is removed from the cytosol primarily by sequestration into the ER by sarco-endoplasmic reticulum Ca^{2+} ATPases (SERCAs) and to a lesser extent by extrusion by plasma membrane Ca^{2+} ATPases out of the cell.

IP_3Rs are spatially organised into clusters with a variable number of channels from 1 to about 15 [33–37]. By including single channels in our cluster definition, we anticipate that the formulated theory will also be applicable to channel populations that do not cluster, as suggested by Lock et al. [37]. The clusters are scattered on the ER membrane with distances reported of 1 to 7 μm [38–42]. CICR and Ca^{2+} diffusion then couple the state dynamics of the channels and clusters. The coupling between channels in a cluster is much stronger than the coupling between adjacent clusters [1].

The structural hierarchy of IP_3R arrangement from single channels to clusters and cellular cluster arrays is also reflected by the dynamic responses of the intracellular Ca^{2+} concentration, as revealed by fluorescence microscopy and simulations [20,38,43–45]. Random openings of single IP_3Rs (blips) may trigger collective openings of IP_3Rs within a cluster (puffs), while Ca^{2+} diffusing from a puff site can then activate neighbouring clusters, eventually leading to a global, i.e., cell-wide, Ca^{2+} spike [20,42,44–46]. Recent studies suggest that clusters generating puffs are preferentially located close to the plasma membrane and single IP_3Rs dominate in the bulk of cells [37,47–49]. The timing of blips, puffs and spikes is random [9,13–17,22,25,26,45,50–52].

The typical spiking time scale is the average T_{av} of ISIs. We learn about processes that generate this time scale by considering the different structural levels. The local dynamics of Ca^{2+} signalling is the dynamics of isolated clusters. Their average interpuff intervals are 1-2 orders

of magnitude shorter than T_{av} [53]. Interestingly, long sequences of puffs from isolated single puff sites do not exhibit slow modulations of the interpuff interval or puff amplitude on the T_{av} time scale [53]. However, interacting puff sites can form spikes; thus, the T_{av} time scale is an emerging property of cell-level dynamics. Once global, these dynamics elicit the negative feedback that terminates spikes. The balance between $[IP_3]$ and the recovery from the negative feedback which terminates spikes determines the length of the stochastic part t_{sto} of ISI. Upon maximal $[IP_3]$, a global elevation of $[Ca^{2+}]_i$ is induced that does not oscillate until the system overcomes its refractoriness.

Stimulation of cells by agonist binding to plasma membrane G protein-coupled receptors (GPCRs) (see Fig 1) activates pathways beyond IP_3 production with receptor-specific feedback to IP_3 levels and Ca^{2+} release [10,32,54–58]. These pathways also affect the negative feedback mechanisms that terminate release spikes. Recovery from this global negative feedback causes the slow increase in open probability during t_{sto}. It may also cause an absolute refractory period immediately after the spike preceding t_{sto} (see Fig 1B) [9]. The negative feedback that determines the time scale of ISIs is different from the feedback that contributes to interpuff intervals (IPIs) and requires global release events.

In our experimental system, binding of carbachol (CCh) to muscarinic GPCRs leads to their activation and stimulation of downstream pathways involving PLCβ isoforms and Protein Kinase C (PKC) [59,60]. PLC catalyses the hydrolysis of phosphatidylinositol 4,5-bisphosphate (PIP_2) into IP_3 and diacylglycerol (DAG) (Fig 1) [59,60]. Several studies report that PKC exerts negative feedback to IP_3-induced Ca^{2+} release [61–64]. PKC activation requires binding of Ca^{2+} and DAG [64]: IP_3 produced by PLC starts Ca^{2+} release in the cytosol, facilitating PKC translocation to the plasma membrane, where it can interact with DAG [64]. PKC phosphorylates and inhibits PLCβ, thereby reducing IP_3 production and exerting its negative feedback on Ca^{2+} release [59,64]. Corrêa-Velloso et al. report an increase in average ISI upon acute inhibition of PKC with ADP-stimulated hepatocytes, while observing no effect of PKC inhibition on average ISI in UTP-stimulated hepatocytes [65]. The authors also describe more complex PKC-mediated feedback affecting spike width.

Our theory exploits the hierarchical structure of Ca^{2+} signalling from single IP_3Rs to clusters and cluster arrays at the cell level. We perceive spike generation as beginning with the opening of a first cluster. We define a cluster as open, if 1 or more of its channels are open. That first opening sequentially recruits more clusters by CICR until almost all available channel clusters are open, forming a global spike. This stochastic process progresses while the cell recovers from the negative feedback that terminated the previous spike. It can be mapped to a random walk with time-dependent transition probabilities on a linear state scheme indexed by the number of open clusters. The ISI distribution is the first passage time distribution from all clusters closed to almost all clusters open shifted by T_{min}. The moments of this distribution can be determined analytically from the solution of a system of difference equations in Laplace space [66]. A proof-of-principle study demonstrated that this theoretical approach is capable of reproducing the basic general properties of Ca^{2+} spiking [67]. However, the theory was limited to the linear dependence of the transition probabilities on the inhibitory variable I that mediates the termination of the spikes by negative feedback.

We generalise the theory to non-linear dependencies on I in this study. This allows for much more realistic rate expressions and offers rules on how to turn biological ideas into stochastic theory. We illustrate this with a newly derived expression for the contribution of CICR to the transition rates and by implementing the dependence of the single-cluster puff rate on $[IP_3]$ measured by Dickinson et al. [35] into our theory. We introduce the calculation of spike amplitude distributions and the joint probability of ISI and spike amplitude. We parameterise our theory with data from HEK293 cells on the SD-T_{av} relation, amplitude

variability, and ISI-amplitude correlation. Powell et al. suggested that ISIs of HEK293 cells obey a Γ-distribution [14]. We show that a Γ-distribution very well approximates our theoretical results.

Results

Mathematical model

Global dynamics of intracellular $[Ca^{2+}]_i$ arise from the collective behaviour of individual channels, spatially arranged in clusters, that cooperate via CICR to generate spikes, as shown in the experimental records in Fig 2.

Our stochastic model tracks the state of the cluster array over time, describing its state by the number of open clusters (see Fig 3). The probability that the cluster array has k open clusters is denoted by P_k. The dynamics of these state probabilities are given by the Master Equation

$$\frac{dP_k}{dt} = \Psi_{k-1,k}P_{k-1} + (k+1)\delta P_{k+1} - (\Psi_{k,k+1} + k\delta)\,P_k, \tag{1}$$

with $k = 0, \ldots, N_t$, $\Psi_{-1,0} = \Psi_{N_t,N_t+1} = 0$ and $P_{N_t+1} = 0$. Open clusters close with rate δ. Clusters open with the rate $\Psi_{k,k+1}$ (Fig 3), which depends on $[IP_3]$ i_p and $[Ca^{2+}]$ c. $[IP_3]$ is part of

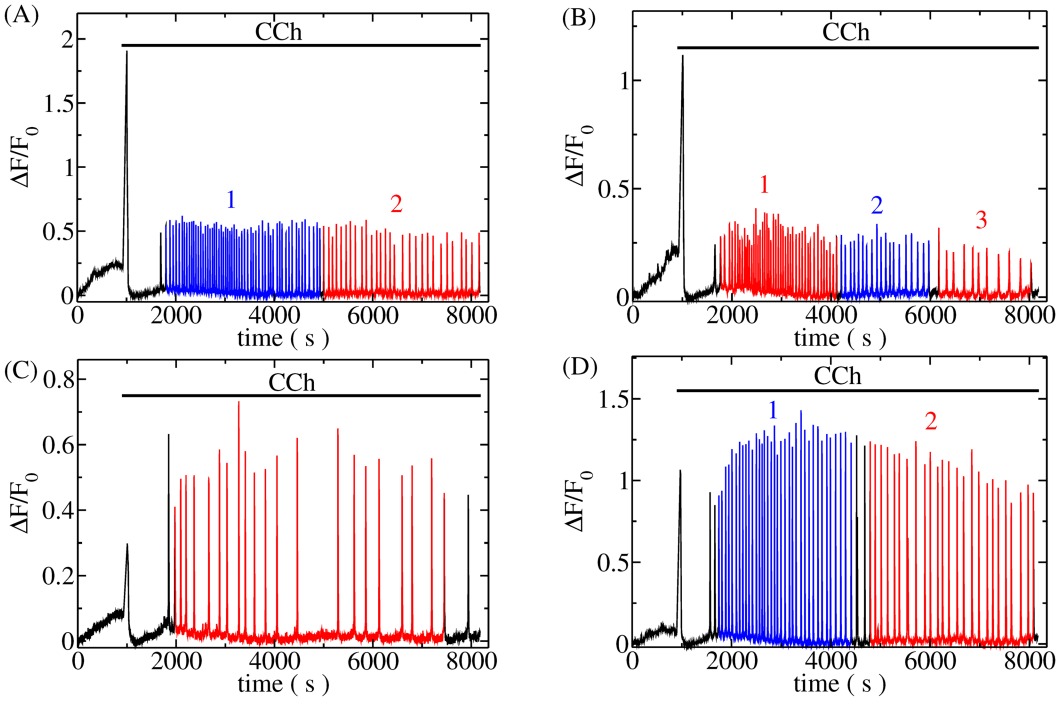

Fig 2. Example recordings of $[Ca^{2+}]_i$ spike trains of HEK293 cells, obtained as described in Sect Materials and methods. Panels A-C are spike trains of three different cells from the same experiment, illustrating cell variability. Panel D displays a cell spike train from a separate experiment with the same conditions as in A-C. All cells were stimulated with 15 μM carbachol (CCh) starting at 900 s. The onset of stimulation triggered an immediate $[Ca^{2+}]_i$ spike, the characteristics of which may depend on the initial Ca^{2+} store state. Colored segments exhibit approximately stationary spiking (see text and Sect D in the S1 Text) and were analysed individually. T_{av} value for A, segment 2 is 111.5 s; B, segment 1 is 54.5 s and segment 3 is 187.5 s; Panel D, segment 1 is 76.2 s and segment 2 is 134.2 s. See also Table 1 for information on other segments.

https://doi.org/10.1371/journal.pcbi.1013322.g002

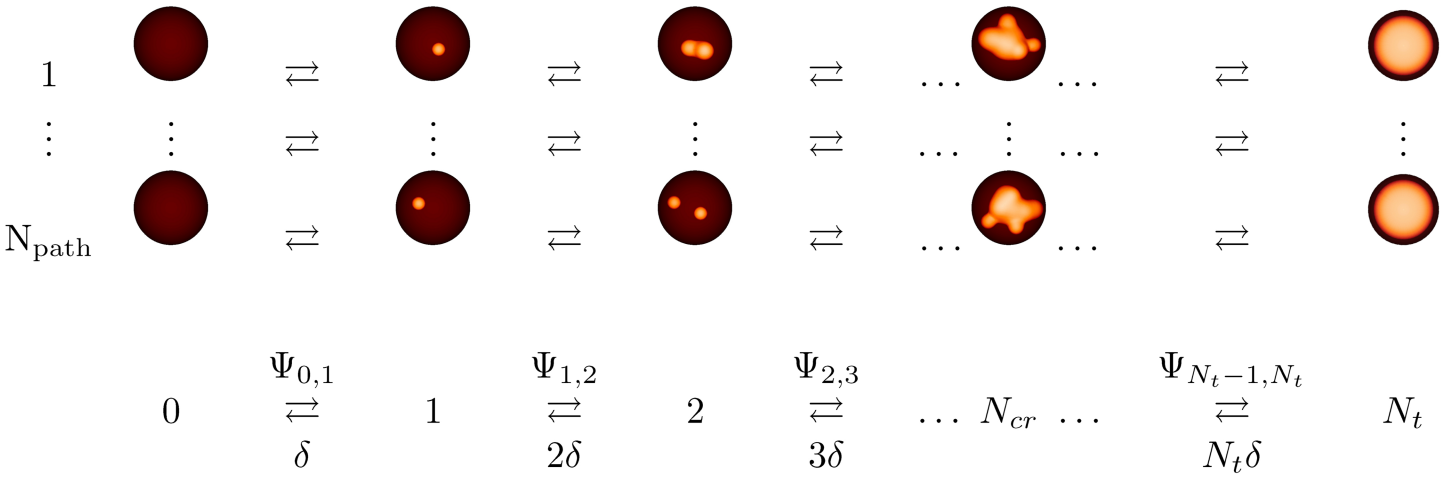

Fig 3. Schematic of cluster array dynamics. (Top) Open clusters are visualised as small orange spheres. A spike occurs when (almost) all N_t clusters are open. There are N_{path} paths of cluster openings and closing from 0 to N_t open clusters. (Bottom) Averaging over all paths leads to a state scheme indexed by the number of open clusters. See text for more explanations.

https://doi.org/10.1371/journal.pcbi.1013322.g003

dynamic feedback and varies with time t. The same applies to $[Ca^{2+}]$ which additionally is affected by the number of open clusters k:

$$\Psi_{k,k+1}\left(i_p, c, t\right) \quad = \quad g\left(i_p(t)\right) \cdot (N_t - k) \cdot r_n(c(k,t)). \tag{2}$$

N_t is the total number of clusters in the cell. The factor $g\left(i_p\right)$ describes the dependency of the single cluster puff rate on $[IP_3]$. $N_t - k$ is the number of closed clusters, and $r_n(c)$ is the rate factor resulting from CICR. The subscript n denotes the number of Ca^{2+} ions required to bind to the IP_3R to be in a state with high open probability.

The time dependence of $\Psi_{k,k+1}$ arises from the recovery of the cell from the negative feedback that terminated the previous spike with rate λ. It aggravates the solving of Eq 1 substantially. Fortunately, the Laplace transform $\tilde{P}_k(s)$ contains most of the information we are interested in. The Laplace transform of Eq 1 is a system of difference equations in Laplace space that can be solved analytically [66,67]. For the analytic solution to be applicable, we had to restrict the transition probabilities to linear dependencies on $e^{-\lambda t}$, which imposed constraints on the modelling of feedback. Here, we generalise the solution to arbitrary polynomial dependencies of the $\Psi_{k,k+1}$ on $e^{-\lambda t}$. The details are given in S1 Text, Sect A. The dependencies of the transition probabilities on $e^{-j\lambda t}, j = 1, \ldots, N_p$ turn the system of first-order difference equations into a system of $N_p th$ order difference equations. We can reduce it to a system of first-order difference equations by the introduction of new variables $\tilde{P}(s)_{jN_t+k}(s) = \tilde{P}(s)_{(j-1)N_t+k}(s+\lambda)$, $j = 1, \ldots, N_p - 1$, and we can solve this system of first-order difference equations by the solution given in [66,67] and Eqs A.8-A.13 in S1 Text. The moments of the ISI distribution are determined by Eqs A.16, A.17. The amplitude distribution is determined by Eqs A.18, A.19. We also simulated trajectories and compared their statistics to the analytical calculations.

The Taylor series illustrates that any function can be approximated by a polynomial. Hence, we can deal with any dependency of the transition probabilities on $e^{-\lambda t}$ now, which we use in this study to introduce more realistic feedback and two concomitant feedback. The Taylor series is usually not the best approximating polynomial for a given polynomial degree

N_p, since its convergence is guaranteed for $N_p \to \infty$ only. We will see below that excellent approximations can be found with a different choice of polynomial coefficients.

The relation between the single cluster puff rate and [IP_3]. Dickinson et al. measured a linear relationship between puff frequency and the number of channels in a cluster [35]. This strongly suggests that channels within a closed cluster behave independently and identically to a very good approximation, and thus the cluster opening probability is proportional to the single channel opening probability.

We now specify the factors on the rhs of Eq 2. The relationship between the single cluster puff rate and a scaled [IP_3] has been measured by Dickinson et al. [35]. [IP_3] has been controlled intracellularly by photo-liberation of IP_3 from an inactive caged precursor in these experiments, and is thus known except for an unknown scaling factor. Consequently, we also use a scaled form i_p of [IP_3], which is scaled with the concentration that saturates the single cluster puff rate. The puff rate measured by Dickinson et al. in SHSY-5Y neuroblastoma cells can be well approximated by

$$g\left(i_p\right) = g_0\left(4.816 i_p - 9.413 i_p^2 + 8.379 i_p^3 - 2.782 i_p^4\right) \tag{3}$$

as shown in Fig 4A. It saturates at $g = 0.937 s^{-1}$ as in SHSY-5Y cells [35] with these coefficients of the polynomial and g_0=1 s^{-1}. The saturation value might be up to 5 times larger in HEK293 cells than in SHSY-5Y cells [53]. [IP_3] is controlled by stimulation with agonist concentration $[A]$. It might also be controlled by the negative feedback that ends the spike, making [IP_3] a dynamic variable. Therefore, we describe i_p during the recovery from negative feedback like

$$i_p = i_p^{max}\left([A]\right)\left(1 - e^{-\lambda t}\right), \quad 0 \le i_p^{max}\left([A]\right) \le 1. \tag{4}$$

Time t = 0 is the end of the absolute refractory period of the previous spike in this equation. At this moment $i_p = 0$ and then recovers to an asymptotic value i_p^{max} set by stimulation with $[A]$.

A spike occurs at the time t_{sto} after the end of the absolute refractory period of the previous spike. Upon onset of the spike, IP_3-targeting negative feedback decreases [IP_3] during the spike and we describe it as follows:

$$i_p \quad = \quad i_p^{max}\left([A]\right) r e^{-\lambda_s t}. \tag{5}$$

The second factor r describes the state of recovery of i_p at the end of the ISI preceding the spike. The cell has recovered to the degree

$$r = 1 - e^{-\lambda t_{sto}} \tag{6}$$

during the ISI preceding the spike. We call r the recovery variable. The last factor is the exponential decrease of i_p with the rate λ_s since the onset of the spike at $t = 0$. This negative feedback to [IP_3] contributes to the termination of the spike.

The rate factor describing CICR. CICR increases the rate of cluster opening, and we derive a corresponding expression for the rate r_n in this section. We focus on the dependency of $r_n(c(k,t))$ on c and k and neglect all factors that can finally be subsumed into a common factor of $\Psi_{k,k+1}$ like g_0 in Eq 3.

We consider the stationary fraction of open channels dependent on [Ca^{2+}] to define ideas about how [Ca^{2+}] affects the channel opening rate. That fraction increases like [Ca^{2+}]^n before

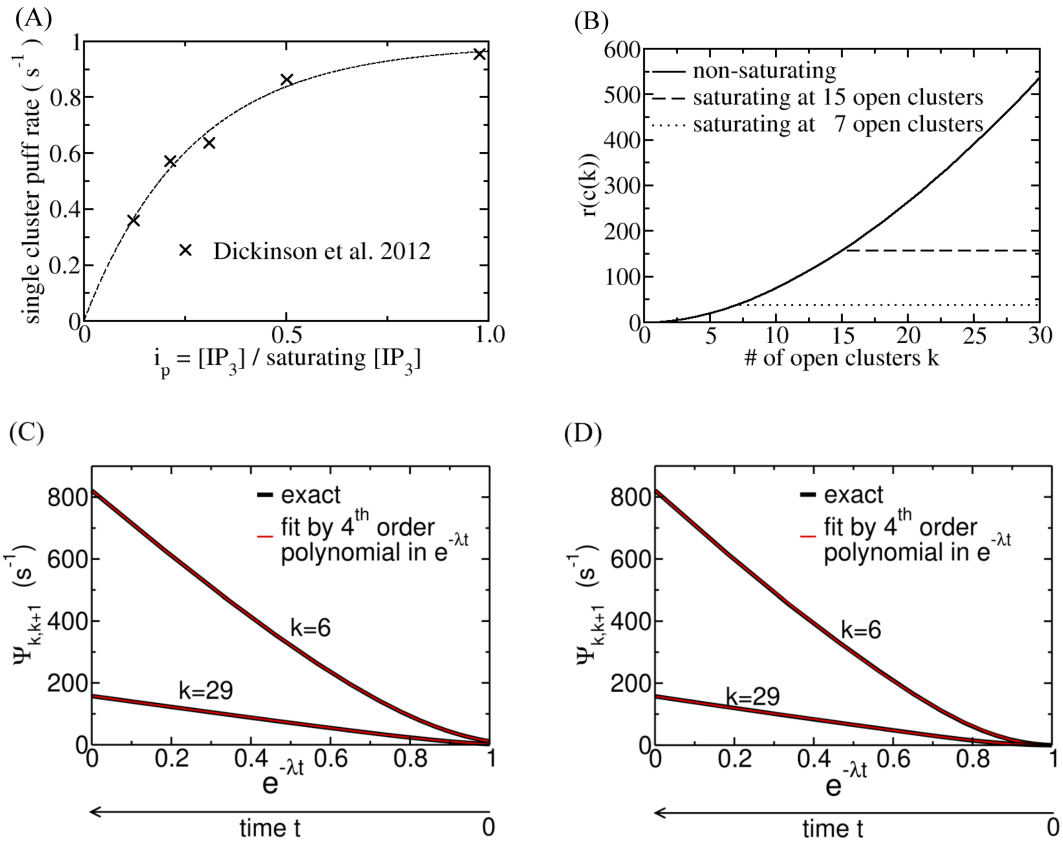

Fig 4. (A) Relation between the single cluster puff rate and [IP$_3$]. Data points from Dickinson et al. [35] are marked by ×. They show a non-vanishing puff rate without uncaging of IP_3 , which might indicate a resting [IP_3]. We shifted the data by this resting concentration. The line is Eq 3. As a remark, $c_0(1 - e^{-c_1 i_p})$ with appropriate values for c_0 and c_1 provides also excellent fits [67] but is not suitable for our analytical calculations. (B) The rate factor describing CICR Eq 10 and Eq 13 fully recovered ($t = \infty$). (C) $\Psi_{k,k+1}$ (Eq 2) in dependency on $e^{-\lambda t}$ with constant [IP_3] ($i_p = 1$) and recovering CICR (Eq 13). (D) $\Psi_{k,k+1}$ (Eq 2) in dependency on $e^{-\lambda t}$ with recovering i_p (Eq 4) and recovering CICR (Eq 13). (C, D) The fits by fourth-order polynomials for each k are indistinguishable from the exact relation. (B-D) $\Delta = 0.95$, $K_p = 18$, $s_p = 2$, $g_0 = 1\ s^{-1}$, $N_t = 30$.

https://doi.org/10.1371/journal.pcbi.1013322.g004

reaching a maximum according to a variety of studies [68–73], with reported values for n from 1.0 to 4.0 (1.0–2.7 [71], 2.7 [68], 1.6 our fit to data from [72], up to 4.0 [70]). That suggests that IP_3R has at least 3 Ca^{2+} ions bound in the state with a high open probability.

Assuming mass action kinetics of Ca^{2+} binding, we can write down a Master Equation for the probabilities $P_b(i)$ that the (tetrameric) IP_3R has i= 0, 1, 2 Ca^{2+} ions bound. We use this Master Equation to calculate the average first passage time (FPT) of the bare receptor to the state with 3 Ca^{2+} ions bound. A standard method of calculating FPT distributions starts with solving the Master Equation with the condition $P_b(3) = 0$ [74]:

$$\begin{aligned} \frac{dP_b(0)}{dt} &= k^- P_b(1) - 4\bar{k}^+ P_b(0) \\ \frac{dP_b(1)}{dt} &= 4\bar{k}^+ P_b(0) + 2k^- P_b(2) - (k^- + 3\bar{k}^+) P_b(1) \\ \frac{dP_b(2)}{dt} &= 3\bar{k}^+ P_b(1) - 2(k^- + \bar{k}^+) P_b(2) \end{aligned} \tag{7}$$

The binding rate constant of Ca^{2+} ions is k^+, and thus $\bar{k}^+ = k^+[Ca^{2+}]$. The dissociation rate is k^-. The Laplace transform of this system of differential equations provides expressions for the Laplace transforms $\tilde{P}_b(i)$ of $P_b(i)$. The average FPT can then be determined from the derivative of $2\bar{k}^+\tilde{P}_b(2)$ as described in S1 Text, Eq C.2. We take the inverse of the average FPT as the rate of reaching the state with 3 Ca^{2+} ions bound:

$$r_3(c) = \frac{12k^+[Ca^{2+}]_r c^3}{13c^2 + 5K_p c + K_p^2}, \quad c = \frac{[Ca^{2+}]}{[Ca^{2+}]_r}, \quad K_p = \frac{k^-}{k^+[Ca^{2+}]_r}. \tag{8}$$

$[Ca^{2+}]_r$ is the resting $[Ca^{2+}]_i$. K_p is the ratio of the dissociation constant of the receptor Ca^{2+} binding site $\frac{k^-}{k^+}$ to $[Ca^{2+}]_r$. If 4 Ca^{2+} ions need to bind to reach the state with high open probability, we obtain:

$$r_4(c) = \frac{12k^+[Ca^{2+}]_r c^4}{25c^3 + 18K_p c^2 + 13K_p^2 c + 3K_p^3}. \tag{9}$$

Another factor of r_n comes from the picture of spike generation as wave nucleation [46,75–78]. We describe it in a very naive approach. The closed clusters near the expanding wave experience high $[Ca^{2+}]$ and dominate cluster opening. Their number increases as the surface of the volume is engulfed by the wave. The number of open clusters k determines that volume. Neglecting the factors subsumed into g_0 we reach the expression:

$$r_3(c) = \frac{c^3 (1+k)^{\frac{2}{3}}}{c^2 + \frac{5}{13}K_p c + \frac{1}{13}K_p^2}. \tag{10}$$

$$r_4(c) = \frac{c^4 (1+k)^{\frac{2}{3}}}{c^3 + \frac{18}{25}K_p c^2 + \frac{13}{25}K_p^2 c + \frac{3}{25}K_p^3}. \tag{11}$$

We choose a simple linear relation between scaled $[Ca^{2+}]$ c and the number of open clusters by assuming quasi-stationary profiles of the cytosolic concentration. They reach their shape in the cytosol quickly upon opening or closing of clusters, but the dynamics of slow variables determining the cytosolic profiles, e.g. the ER filling state, slowly change the cytosolic concentration even with a constant configuration of open clusters [1,2,79].

The model $[Ca^{2+}]$ concentration variable c is the concentration in units of the resting concentration (Eq 8). It is an increasing and saturating function of the number of open clusters [1,2,79,80]. We set $c = 1 + kS_p(t)$. $S_p(t)$ quantifies how much a single open cluster increases c (in units of $[Ca^{2+}]_r$). If many but not all clusters are open, $[Ca^{2+}]$ is high at most closed clusters. The opening of more clusters will not increase $[Ca^{2+}]$ further for most closed clusters, since they are most likely not proximally localised to those that are opening. Hence, we describe saturation by limiting c to values reached at the number k_s of open clusters

$$c(k,t) = \begin{cases} 1 + kS_p(t) & , \quad k \le k_s \\ 1 + k_s S_p(t) & , \quad k \ge k_s \end{cases}. \tag{12}$$

The upper bound k_s applies also to the factor $(1+k)^{\frac{2}{3}}$ in Eqs 10, 11 and thus in the end fixes an upper bound to $r_n(c)$ (Fig 4).

$S_p(t)$ picks up the slow dynamics. We exemplify our ideas with ER depletion. The ER is (partially) depleted at the end of a spike, the release currents are reduced, and thus S_p is decreased. Furthermore, the luminal Ca^{2+} controls the IP_3R gating [81]. We describe depletion by a factor $1 - \Delta$, $0 \le \Delta \le 1$. The degree of depletion may be minor, causing little decrease

in release rates and S_p ($\Delta \ll 1$) or may cause a substantial decrease of S_p ($\Delta \approx 1$). The ER slowly refills after the spike, i.e. the depletion factor approaches 1: $S_p(t) = s_p\left(1 - \Delta e^{-\lambda t}\right)$. That leads to an expression for c during recovery from depletion like

$$c(k,t) \quad = \quad 1 + ks_p\left(1 - \Delta e^{-\lambda t}\right). \tag{13}$$

The ER depletes during a spike, and thus we get

$$c(k,t) = 1 + ks_p\left(1 - \Delta\left(1 - re^{-\lambda_s t}\right)\right). \tag{14}$$

with t = 0 being the time of onset of the spike.

The time dependent c (Eq 13 or 14) enters $r_n(c)$ (Eq 10 or 11) and thus causes a dependency of the $\Psi_{k,k+1}$ (Eq 2) on $e^{-\lambda t}$: $\Psi_{k,k+1}\left(i_p, c\left(k, e^{-\lambda t}\right), k\right)$. That dependency is shown in Fig 4C. It can be very well approximated by a fourth-order polynomial in $e^{-\lambda t}$.

Combining negative feedback to [IP_3] and ER depletion. Since each spike partially depletes the ER, this negative feedback is always present. Therefore, negative feedback to [IP_3] always occurs in combination with ER depletion, and the $\Psi_{k,k+1}$ depend on $e^{-\lambda t}$ via c (Eqs 10, 11 and 13, 14) and i_p (Eq 3 and Eqs 4, 5): $\Psi_{k,k+1}\left(i_p\left(e^{-\lambda t}\right), c\left(k, e^{-\lambda t}\right), k\right)$. This complex dependency on $e^{-\lambda t}$ can also be well approximated by a fourth-order polynomial, as Fig 4D shows. The reasons for the high quality of these fits are that $e^{-\lambda t}$ only varies between 0 and 1, that the functions we deal with are smooth, and that we fit up to the saturating argument value, but not far into the saturated range.

In summary, we can find polynomial expressions capturing the time dependency of feedback for all the cases we considered, and thus we can broadly apply our analytic theory. This allows for a much larger variety of models than before [67]. We used the combined feedback throughout this study.

The ISI distribution and its moments

The first step in determining the ISI distribution is to define what a spike is. Some cells exhibit release events larger than puffs, but still much smaller than spikes: the number of open clusters here is too small, and CICR has not yet reached the strength necessary to convert those events into global spikes. If the number of open clusters is large enough, CICR opens clusters in a fast sequence during the rising phase of the spike. We call a release event a spike if it is of size k_{sp}, which is large enough to cause this fast rise. Since the upstroke is fast, the distributions of FPTs t_f to numbers of open clusters k larger than k_{sp} are very similar. Thus, we can determine k_{sp} as the smallest k in a sequence of ks with similar t_f-distributions. We consider as a spike all release events with at least k_{sp} open clusters. The results in Fig 5A and 5B suggest $k_{sp} = 7$ to meet the definition. The distribution of t_{sto} is the distribution of FPTs from 0 to k_{sp} open clusters with this definition of a spike.

We show several examples of simulated ISI distributions with a varying Ca^{2+} dissociation constant of IP_3R in Fig 5C. The larger the dissociation constant K_p the less likely it is that the receptor has 3 Ca^{2+} ions bound at a given $[Ca^{2+}]_i$, and the larger $[Ca^{2+}]_i$ transients are required to generate a spike. It takes larger opening probability $\Phi_{k,k+1}$ to generate these transients, which occurs later in the recovery process than the one required with small K_p. Thus, the average ISI T_{av} increases with increasing K_p. The Ca^{2+} sensitivity is regulated by ATP [71,82–85]. The IP_3R-subtype 1 is about 3 times more sensitive in elevated [ATP] than in low [ATP], and the subtype 3 is about 10 times more sensitive. Our results suggest that a lack of ATP and a consequential decrease in the Ca^{2+} sensitivity increase the average ISI. This is

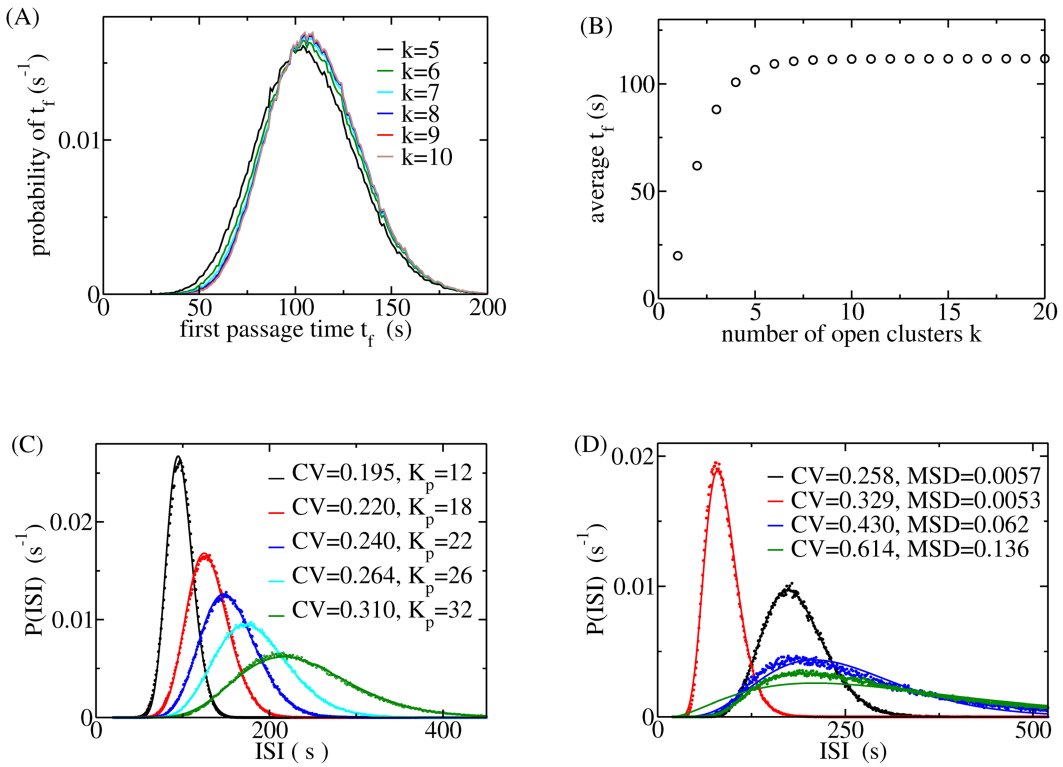

Fig 5. (A) The distributions of the FPT t_f from 0 to k open clusters. They are very similar for k = 6-10. (B) The average of the FPT t_f from 0 to k open clusters. The value of t_f at k = 7 (110.5 s) deviates by about 1% from the values wit k≥15 (111.6 s). Based on that criterion, we will use $k_{sp} = 7$ in our calculations of spike characteristics. (C) ISI distributions with varying Ca^{2+} dissociation constant K_p of the IP_3R. CV is the coefficient of variation of the stochastic part of the ISI. The T_{av} values with increasing K_p are 77 s, 110 s, 135 s, 164 s and 217 s. (D) ISI distributions can be very well approximated by Γ-distributions if the CV is sufficiently small. We find an excellent or good approximation for CV ≤ 0.43, but not for CV = 0.614. MSD is the mean root of the squared deviation relative to the maximum of the Gamma distribution. (A, B, D) $\Delta = 0.95$, $N_t = 30$, $s_p = 2$, $k_s = 15$, $K_p = 18$, $g_0 = 1.0\ s^{-1}$, $i_p^{max} = 0.1$, $\lambda = 0.01\ s^{-1}$, (D) parameter values different from the common set: black $g_0 = 0.6\ s^{-1}$, red $g_0 = 0.2\ s^{-1}$, $i_p^{max} = 0.75$, $\lambda = 0.02\ s^{-1}$, blue $g_0 = 0.3\ s^{-1}$, $\lambda = 0.02\ s^{-1}$, green $K_p = 32$, $g_0 = 0.6\ s^{-1}$, $\lambda = 0.02\ s^{-1}$.

https://doi.org/10.1371/journal.pcbi.1013322.g005

in agreement with experiments by Betzenhauser et al. in DT40 cells investigating the properties of IP_3R II [85]. They observed an increase in ISI and a decrease in spike amplitude upon mutating the relevant ATP-binding site on IP_3R. Thus, cell-to-cell differences of [ATP] may be another parameter causing cell variability of the average ISI T_{av} besides parameters including number of clusters, specific geometry of the cluster array, density of plasma membrane receptors, SERCA density and more (see [67,86] for detailed discussions).

Powell et al. found that the experimentally determined ISIs of HEK293 cells obey Γ-distributions [14]. Therefore, we compare our simulated distributions with Γ-distributions with the same average and SD (Fig 5D) and find very good agreement.

We can relate the experimental results to the theoretical ISI distributions via moments, cumulants, their relationships and the coefficient of variation CV (CV = SD/average). The CV of the stochastic part of the ISI is well approximated by the slope of the cumulant relation between the average of the ISI T_{av} and the ISI SD σ

$$\sigma = \alpha\,(T_{av} - T_{min})\,. \tag{15}$$

It is of particular interest, as we found that it is conserved despite the large variability in T_{av} and σ between cells under identical conditions and also in a variety of experimental situations [9,13]. That robustness is important since the smaller the value of α, the larger the information content transmitted by a spike sequence measured either as Kullback entropy with a Poisson distribution as reference [87,88] or mutual information between stimulating agonist concentration and T_{av} [89]. The Γ-distributions describing the HEK293 ISI statistics are two-parameter distributions with a shape and a rate parameter. The shape parameter is equal to CV^{-2} and is consequently as conserved as α and the same for all individual HEK293 cells in many different experimental situations [9,13].

There are two experimental observations related to α - its value for ISI in the range of $T_{av} \approx \lambda^{-1}$, and the robustness of this value against cell variability. Both require some reflection. Recovery from negative feedback during the first passage process of spike generation is the reason why α has a value smaller than 1.0. The absence of recovery or very fast recovery, that is, $\lambda \gg T_{av}{}^{-1}$, entails $\alpha = 1.0$ [74,87,88]. From these considerations, it is clear that the rate of recovery from negative feedback λ sets the slope α of the cumulant relation Eq 15 [67,90].

If T_{av} is very large, i.e. $T_{av} \gg \lambda^{-1}$, recovery is fast compared to T_{av} and α has values close to 1. Consequently, the T_{av} range through which we measure a typical value of α is another characteristic of the pathway. That defines the robustness requirements. The value of α should be approximately constant throughout the range of observed average ISI, and experiments suggest that this range is much larger than the smallest ISI [9,13].

We are now in a position to assess our theoretical results and relate them to experimental observations. We show the results of calculations for the CV of the stochastic part for a range of K_p values for average ISI up to 400 s (Fig 6A). CV is moderately affected by K_p. It shows a much stronger dependency on T_{av} with $\lambda = 0.01\ s^{-1}$ than with $\lambda = 0.005\ s^{-1}$. Therefore, we used $\lambda = 0.005\ s^{-1}$ in fits of our HEK293 data to capture the T_{av}-range with approximately constant CV. Interestingly, CV exhibits a minimum in relation to T_{av} both in theoretical and experimental results.

We measured $[Ca^{2+}]_i$ spike trains in HEK293 stimulated with Carbachol (CCh) as described in Materials and methods. Stationary segments of spike trains as shown in Fig 2 were analysed with regard to ISI and amplitude sequences, from which we calculated averages and SDs.

We obtain a value of α from our experimental data by fitting it to the population data (Fig 6B). The plot of individual ISI SD- and T_{av}-data points of all cells reproduces the cumulant relation Eq 15. Fitting the linear function across the whole T_{av} range provides $\alpha = 0.231$. Restricting the fit to ranges of small, intermediate and large values of T_{av} as specified in the caption of Fig 6B shows that we find a minimal α in the experimental data, which is consistent with our theoretical results (Fig 6A). We measured values of α in the range from 0.2 to 0.26 for HEK293 cells in an earlier study [9]. Here, we find values between 0.219 and 0.280, in agreement with the earlier results.

The amplitude distribution

The spike amplitude is the maximum of open clusters reached during a spike. It is at least k_{sp} due to the definition of a spike. The distribution $P(A|r)$ of amplitude A is affected by the degree of recovery r (Eq 6) at the spike time. We calculate $P(A|r)$ from the probabilities that given a spike (initial state $k = k_{sp}$), the process reaches $A > k_{sp}$ before reaching 0. These splitting probabilities are determined by setting both 0 and A as absorbing states. Sect A of S1 Text explains the details. $P(A|r)$ is the difference between the sequential splitting probabilities for

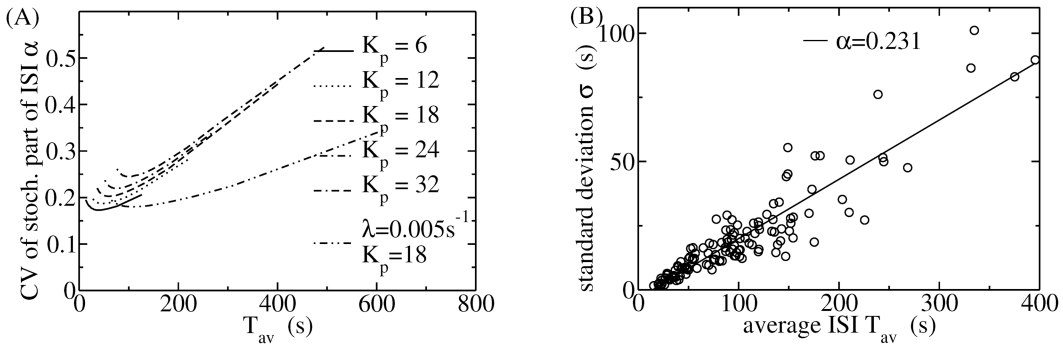

Fig 6. (A) The relationship between the CV of the stochastic part of the ISI α and T_{av} for a variety of K_p- values. The range of T_{av}-values of the data is caused by varying i_p^{max} from 0.025 to 1.0. α stays within the measured range of HEK cells with $\lambda = 0.005$ s^{-1}. Parameter values $\Delta = 0.95$, $N_t = 30$, $s_p = 2$, $k_s = 15$, $g_0 = 1.0$ s^{-1}, $\lambda = 0.01$ s^{-1} if not indicated otherwise. Eq 10 has been used for CICR. (B) The cumulant relation Eq 15 was measured with HEK293 cells. Each data point represents results from one spike train. The slope α of the cumulant relation approximates the CV of the stochastic part of the ISI. The full line is a fit of a linear function to all data points with the indicated α-value. Fitting linear functions to the ranges $0 \le T_{av} \le 70$ s, 70 s $\le T_{av} \le 160$ s and 160 s $\le T_{av} \le 400$ s provides slopes of 0.262. 0.219 and 0.280, i.e. we find a similar non-monotonic behaviour as in theory.

https://doi.org/10.1371/journal.pcbi.1013322.g006

reaching A. We verify this method of calculating the amplitude distributions by simulations in Fig 7A. Simulations and analytical calculations are indistinguishable.

If a spike occurs shortly after the previous one, the cell has only slightly recovered from the negative feedback that terminated the previous spike. The cluster open probability is small and the probability that the amplitude is larger than k_{sp} is negligible. Conversely, with almost complete recovery ($r \approx 1$), the cluster open probability is large and the probability of observing small amplitudes becomes insignificant. The dependency of P(A|r) on r connects P(A|r) to the ISI distribution $P(ISI)$.

Once the spike has started, the negative feedback, which will terminate it, starts to grow with rate λ_s (Eqs 5, 14). That rate has a moderate effect on the amplitude distribution (Fig 7B). The slower the negative feedback grows, the larger the spike amplitude. Since typical spike

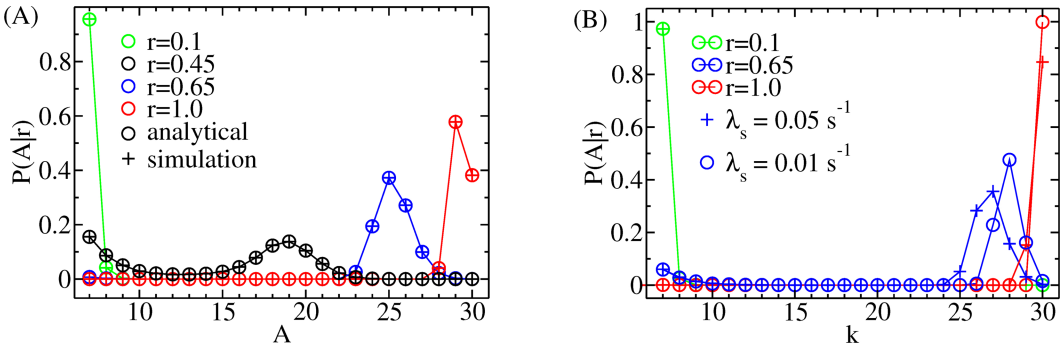

Fig 7. Amplitude distributions. We show the probability P(A|r) that A open clusters are reached during a spike given that $k_{sp} = 7$ clusters are initially open, i.e. given the release event is a spike. A is a discrete variable; the lines are only a guide for the eye. (A) P(A|r) is affected by the degree of recovery r from negative feedback at the time of the occurrence of the spike. (B) The rate of growth of the negative feedback during the spike also affects P(A|r) (Eqs 5, 14). (A, B) $\Delta = 0.95$, $K_p = 18$, $s_p = 2$, $N_t = 30$, $i_p^{max} = 0.1$, (A) $k_s = 10$, $g_0 = 1$ s^{-1}, $\lambda_s = 0.05$ s^{-1}, (B) $k_s = 15$, $g_0 = 0.6$ s^{-1}.

https://doi.org/10.1371/journal.pcbi.1013322.g007

durations are in the range of 20 s, we use $\lambda_s = 0.05\ s^{-1}$ in this study. In a future study, a detailed investigation of the role of λ_s will be carried out in the context of spike modelling.

The joint ISI-amplitude distribution P(A,ISI)

We calculate the probability of a spike with amplitude A_{i+1} following the *ith* ISI_i in this section. We can transform $P(A|r)$ by $r = 1 - e^{-\lambda t_{sto}}$ and $ISI = T_{min} + t_{sto}$ into P(A|ISI). The joint probability is P(A,ISI) = P(A|ISI)P(ISI). We drop the indices of A and ISI in the distribution arguments for convenience of notation. Fig 8 shows examples of P(A,ISI). We calculated P(A|ISI) (see S1 Text, Eqs A.18, A.19 and A.21) and the moments of the ISI distribution (see S1 Text, Eq A.16 and A.17) analytically and then used Γ-distributions for P(ISI). We see distributions with high correlation between ISI_i and A_{i+1} (Fig 8A) and weak correlation (Fig 8D). We get maximum-amplitude spikes across almost the whole ISI range in the case of weak correlation. Correlated spike trains show small-amplitude spikes at short ISI and large amplitudes at long ISI.

We cannot directly verify the joint probability distribution with experimental data since that would require extremely long spike sequences. We therefore examine the correlation between ISI_i and subsequent amplitude A_{i+1}, instead. Fig 9A shows A_{i+1} plotted against ISI_i

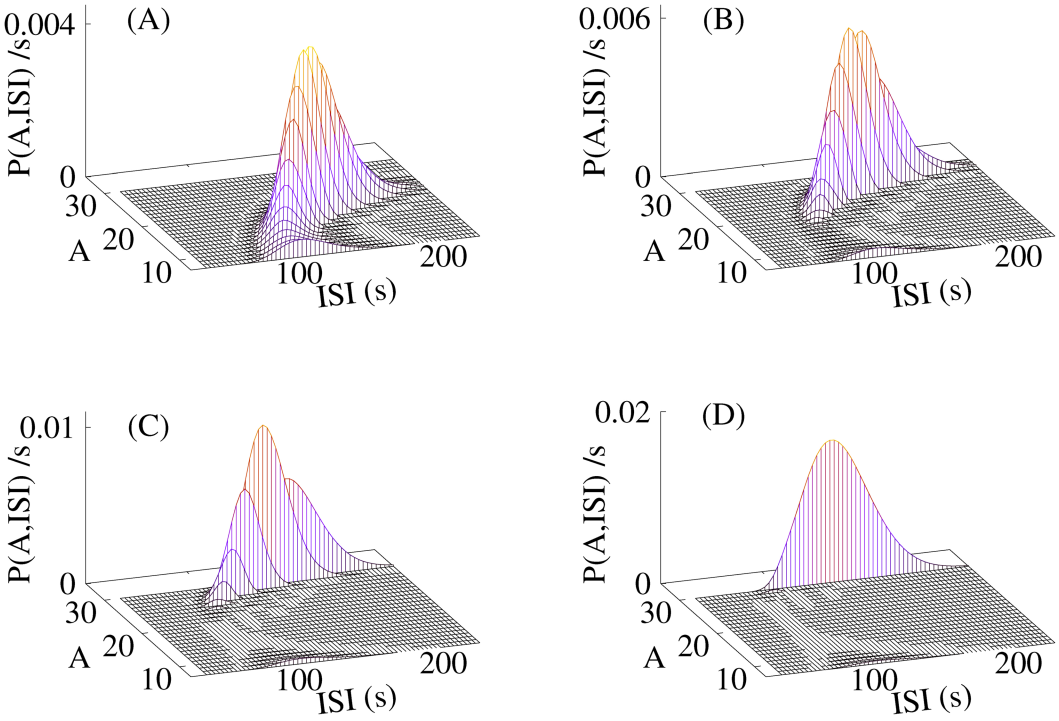

Fig 8. The joint ISI-amplitude distribution P(A,ISI) is the probability of observing a spike with amplitude A when the time ISI has passed since the onset of the previous spike. The number of open clusters k_s at which the CICR factor saturates has been increased from (A) to (D) to obtain distributions with different values of the correlation coefficient C_c (see Eq 12). Small amplitude spikes occur with some probability at small k_s early in the ISI (A). Essentially all-or-none spikes occur at large k_s values, only (D). Panel A shows a distribution typical for high correlation $C_c = \langle ISI_i | A_{i+1} \rangle$ between ISI_i and subsequent amplitude A_{i+1}. Panel D is typical of low correlation. (A) $k_s = 6$, $C_c = 0.755$, (B) $k_s = 10$, $C_c = 0.589$, (C) $k_s = 15$, $C_c = 0.396$, (D) $k_s > N_t$, $C_c = 0.213$, (A-D) $\Delta = 0.95$, $K_p = 18$, $s_p = 2$, $g_0 = 1\ s^{-1}$, $N_t = 30$, $i_p^{max} = 0.1$, $\lambda = 0.01\ s^{-1}$. Eq 10 has been used for CICR.

https://doi.org/10.1371/journal.pcbi.1013322.g008

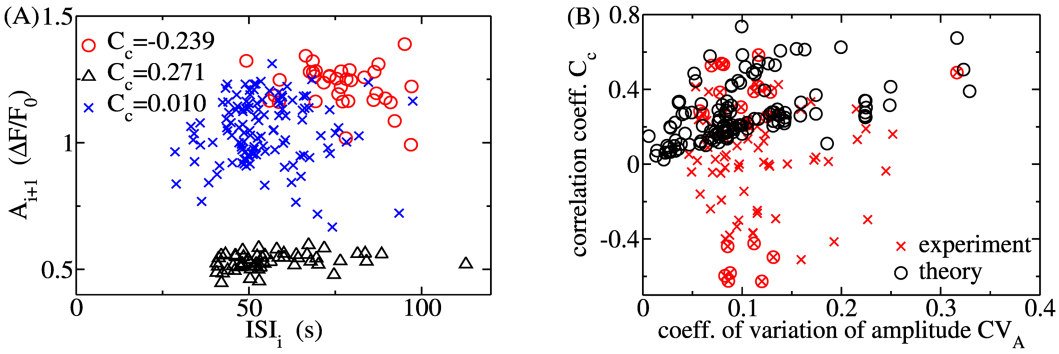

Fig 9. The relation of the *ith* ISI_i and the subsequent spike amplitude A_{i+1}. (A) A_{i+1} versus ISI_i for typical spike trains with negative, positive, and vanishing Pearson correlation coefficient C_c. All three of them exhibit weak or no correlation. (B) Pearson correlation coefficient C_c versus the coefficient of variation of the amplitude CV_A from theory with 136 parameter value sets and for all (36) measured spike trains with at least 15 ISIs. Each black and red data point represents a measured or simulated spike train, respectively. The C_c of encircled experimental data points has a p-value <0.05. Our theory provides only positive values of C_c. The parameter values for the simulations and calculations are $\Delta = 0.95$, $g_0 = 40\ s^{-1}$ $\lambda = 0.005\ s^{-1}$, all other parameter values have been varied, Eq 9 has been used.

https://doi.org/10.1371/journal.pcbi.1013322.g009

for HEK293 spike trains with negative, positive, and vanishing correlation coefficients. These plots suggest a lack of a well-defined relationship between ISI_i and A_{i+1}.

Panel B of Fig 9 provides a more comprehensive analysis. It shows the Pearson correlation coefficients $C_c = \langle ISI_i | A_{i+1} \rangle$ and the coefficient of variation of the amplitude CV_A for spike trains measured with more than 15 spikes and theoretical results. The measured spike trains exhibit positive and negative C_c with absolute values ranging from 0.034 to 0.615. The p-values of most of the correlation coefficients are larger than 0.05. We encircled those with p-values smaller than 0.05, among which we find values close to 0.6, -0.6, and 0.22, i.e. correlation between ISI_i and A_{i+1}, anticorrelation, and lack of correlation. Fig 9B shows that theory reproduces the range of positive values.

Our theory formulates the idea that the recovery from the negative feedback that terminated the previous spike increases the IP_3R open probability or spike amplitude with increasing ISI. Consequently, it produces only positive C_c for ISI_i and A_{i+1}. We find both correlation ($C_c \approx 0.6$) and lack of correlation ($C_c < 0.25$) in our calculations and experiments. Hence, contrary to our expectations, recovery from negative feedback does not necessarily cause a correlation between ISI_i and A_{i+1}.

There are experimental spike trains that exhibit vanishing C_c in a wide range of CV_A and T_{av}. Theoretical C_cs vanish only at small values of CV_A or at very large T_{av} ($T_{av} \gg \lambda^{-1}$, see the black circle at CV≈0.2 and $C_c \approx 0$ in Fig 9B). This observation, together with the negative correlation coefficients found in our experiments, is a strong indication of processes affecting the correlation between ISIs and amplitudes, which are not included in our theory, yet.

Remarks on quantifying parameter values in the face of large cell variability

IP_3-induced Ca^{2+} spiking shows characteristics that are not subject to cell variability, such as α and the agonist sensitivity γ of the concentration-response relation of T_{av} [9], and spike train properties like T_{av}, the ISI SD σ, amplitudes and C_c with large cell variability. This entails a corresponding set of parameter values that most affect variable properties (N_t, s_p, k_s, K_p) and thus quantify cell variability and another set of parameters relating to 'conserved' values.

The latter are λ and g_0 in our theory, due to the properties of α. Note that the value of γ is not restricted by the current level of theory and therefore can always be met.

The purpose of theory is to reproduce both the values of the conserved properties and the value ranges of the variable properties, and thus to provide a quantitatively consistent formulation of a mechanistic hypothesis of spike generation including both. Theory should also be able to reproduce results for a specific set of variable properties of a given cell by specifying the values of parameters that describe cell variability. Table 1 shows three examples that we can also fit individual cells. Those example cells have been chosen to have more than 15 spikes, positive C_c, and to represent short, intermediate and long T_{av}. We specify all parameter values for the three cells in the table. We used the value of α, its robustness properties, and the T_{av} range to specify λ, g_0 and the range of K_p. We used T_{av}- and C_c-values to quantify the parameters describing cell variability. It was easier to fit the robustness properties of α and the properties of the specific cells in Table 1 when we used Eq 11 instead of Eq 10.

Discussion

We present a stochastic model of IP_3-induced Ca^{2+} spiking in HEK293 cells and parameterise it through experiments. The model takes into account the slow deterministic behaviour of globally averaged feedback variables. Transition probabilities depend non-linearly on the feedback variables. Analytical theory required to find a method to solve the corresponding time-dependent Master Equation. We generalised a linear method [66] to a polynomial dependency by reducing a system of higher-order difference equations to a system of first-order difference equations. The generalisation now allows for a very broad spectrum of dependencies of transition probabilities on the state of the system and dynamic feedback variables.

We calculate the first and second moments of the ISI distribution analytically. Since simulated ISI-distributions with α-values applying to HEK293 cells are very well approximated by Γ distributions in agreement with experimental results [14], we can completely determine ISI statistics analytically. The same applies to the amplitude statistics. That puts us in the position to calculate ISI-amplitude correlations analytically, which we can also determine from measured spike sequences. Hence, our approach substantially expands the possibilities to relate analytical calculations to experimental results.

We derived transition rate expressions for CICR and sensitisation of IP_3Rs by $[IP_3]$. The dependency of the puff rate on $[IP_3]$ has been measured by Dickinson et al. [35] and we used

Table 1. Fits for three example spike trains from Fig 2. Parameter values: Fig 2A, segment 1: $K_p = 23$, $k_s = 10$, $s_p = 2.75$, $i_p^{max} = 1.0$; Fig 2B, segment 2: $K_p = 22$, $k_s = 13$, $s_p = 1.19$, $i_p^{max} = 0.73$; Fig 2C: $K_p = 18$, $k_s = 14$, $s_p = 0.61$, $i_p^{max} = 0.118$. The parameter values common to all three cells are $N_t = 30$, $\Delta = 0.95$, $g_0 = 40\ s^{-1}$ $\lambda = 0.005\ s^{-1}$. Eq 11 has been used for CICR. The units of T_{av} and T_{min} are seconds. The values for T_{min} are estimates from the experimental records. The theoretical T_{min}-values are parameters and not results of calculations. Experimental values of α of individual cells cannot be determined since we do not know individual T_{min}-values. N_{sp} is the number of spikes. Theoretical results are moments of distributions which do not have N_{sp} as parameter (n.a.).

	Fig 2A, segment 1		Fig 2B, segment 2		Fig 2C	
	exp.	theo.	exp.	theo.	exp.	theo.
T_{av}	56.7	56.5	97.9	97.6	238.9	236.4
C_c	0.271	0.276	0.215	0.206	0.296	0.287
CV_A	0.060	0.049	0.093	0.096	0.129	0.143
α		0.222		0.193		0.185
N_{sp}	57	n.a.	19	n.a.	20	n.a.
T_{min}	15	15	20	20	20	20

https://doi.org/10.1371/journal.pcbi.1013322.t001

their results (Eq 3). The CICR factor has been derived as the inverse of the first passage time from the bare receptor to the state with either 3 or 4 Ca^{2+} ions bound (Eqs 10, 11). Furthermore, we can now simultaneously include several time-dependent feedback. Each feedback may have its own relaxation rate, as long as the ratio of rates is a rational number.

That implicates progress toward a theory closer to the experiment. The parameter values, which we obtain as part of the results of the theory, now correspond more to expectations based on average ISIs. For example, the rate of recovery from negative feedback λ sets the slope α of the cumulant relation Eq 15 [67,90]. The fit of earlier experimental data with our previous models resulted in $\lambda = 1.44\ s^{-3}$ [67]. Such a recovery time of about 700 s was required to meet the robustness properties, but it appears rather long compared to average ISIs. In those earlier models, we used a simple power function dependency of the CICR factor on the number of open clusters. With time-dependent $[Ca^{2+}]_i$ and our current description of CICR by Eqs 10 and 11, the new parameter K_p is part of the description of CICR. It also affects α. This additional degree of freedom in fixing α allows more realistic values of λ (Fig 6A). The measured α-values in this study agree very well with earlier measurements [9]. That confirms our conclusion that the slope of the cumulant relation is a characteristic feature of spike trains elicited via a specific GPCR in a given cell type, that α is robust against many perturbations and is not subject to cell variability.

We found better agreement of α robustness properties and correlation coefficients with the expression of the CICR factor assuming binding of 4 Ca^{2+} ions to reach high open probability (Eq 11) than with binding of 3 ions. Both expressions, Eq 10 and Eq 11, are essentially linear for large $[Ca^{2+}]$. Interpretation of this result needs to take into account that CICR may include Ca^{2+} dependencies in addition to the mass action kinetics we included here as, for example, the IP_3R modelling study by Siekmann et al. illustrates [72]. The assumption that 4 ions need to bind entails a very small transition probability at small $[Ca^{2+}]$, which then rises quickly with increasing $[Ca^{2+}]$. It thus entails a sharper threshold of spike initiation compared to the binding of 3 ions. Our results suggest highly non-linear rate expressions with sharp thresholds to correspond to experimental observations. However, this highly non-linear behaviour of cells might not be due to mass action kinetics alone.

The experimental and theoretical results for the Pearson correlation coefficient C_c are, to some degree, unexpected. Expectations are shaped by the ideas on feedback during a spike sequence, which defines our theory. Upon onset of a spike, negative feedback is initiated, e.g. by ER depletion or diminution of IP_3 production, and finally terminates the spike. Afterwards, the cell recovers from it, which causes a continuous increase of the spike probability up to some saturation value. This suggests a correlation between an ISI and the amplitude of the subsequent spike. Some spike trains exhibit such a correlation ($C_c \geq 0.4$). However, many more show weak correlation ($0.25 \leq C_c \leq 0.4$), no correlation ($|C_c| \leq 0.25$), or even anticorrelation ($C_c \leq -0.25$). These correlation properties are subject to cell variability, i.e. HEK293 cells stimulated identically can exhibit any of the four cases. This suggests that correlation is not only a characteristic of feedback triggered by muscarinic receptor activation, but is also strongly affected by cell-specific properties, which are subject to cell variability.

A negative ISI-amplitude correlation could be explained by decreasing IP_3R open probability at large ISI due to a very slowly decaying positive feedback component during the spike. However, that would substantially increase α in Eq 15 away from measured values [88]. The challenge, therefore, is to find feedback mechanisms providing both $C_c < 0$ and $\alpha \ll 1$. The analytical stochastic theory presented in this study, will be of value for testing hypotheses on the pathway components that cause this anticorrelation since it can include a large variety of positive and negative feedback mechanisms.

In general, mathematical theory is a formulation of our mechanistic and quantitative hypotheses on the system under consideration. Here, we parametrise the model using both general statistical properties and robustness properties. In addition, we specified it to spike trains from three representative cells. However, the resulting parameter sets for the specific spike trains in Table 1 may not be unique. Identifiability in such systems requires at least as many independent single-cell experiments as there are parameters to estimate, each yielding sufficiently long spike trains for robust moment statistics. This is not practically achievable, as the cell state does not remain constant over such a long time (see Fig 2), thereby limiting the ability to formulate a complete hypothesis.

These constraints raise a broader question: What can be inferred about a stochastic, highly variable biological system, and what level of resolution is necessary for functional understanding? While a complete quantitative theory tailored to individual cells could offer detailed insights, its utility is constrained by the high degree of cell variability. In contrast, the robustness of function across heterogeneous cells suggests that essential system behaviours are governed by invariant properties rather than cell-specific parameters.

Theoretical frameworks that incorporate stochasticity and biological variability - while remaining faithful to function and the general statistical features of the system - may not be fully predictive at the single-cell level. However, they can still elucidate the core design principles that ensure functional robustness. Such an approach may help distinguish biological systems from engineered technological systems, the former being characterised by resilience to parameter variability, the latter requiring precise composition. In the long term, incomplete yet principled models of this nature may provide critical insights into the architectural logic of living systems.

Materials and methods

Materials

Dulbecco's Modified Eagle's Medium (DMEM) supplemented with 4.5 g/L D-glucose and L-glutamine, and FluoroBrite DMEM were from Thermo Fisher Scientific. Calbryte™ 520 AM was purchased from AAT Bioquest, and carbamoylcholine (carbachol; CCh) was sourced from Merck (Sigma-Aldrich). 35 mm glass-bottom dishes for imaging were from ibidi GmbH.

Single-cell imaging of $[Ca^{2+}]_i$ in HEK293 cells

HEK293 cells were cultured in DMEM supplemented with 10% fetal bovine serum (FBS). For imaging experiments, the cells were plated onto 35-mm glass-bottom petri dishes; loaded with CalBryte™ 520 AM (2.5 μM) for 30 minutes at 37 °C , washed with fresh DMEM, and incubated again for an additional 30 minutes before imaging to allow for de-esterification of the indicator. Single-cell fluorescence measurements were performed at 30 °C under humidity and 5% CO_2 control in conditioned FluoroBrite DMEM supplemented with 10% FBS and 4 mM L-glutamine to better preserve cell viability during the extended acquisition. CCh was added to the cells by pipette 15 minutes after the recording started at varying concentrations (3 μM , 5 μM , 10 μM , and 15 μM) across different experiments. Cells were imaged using a Nikon inverted microscope equipped with a spinning disk unit (ANDOR CSU-W1) featuring a 50 μm fixed-size pinhole. A Plan Fluor 20x Mimm DIC N2 objective (NA 0.75) was used for image acquisition. Detection was carried out using an Andor iXon DU-888 EMCCD camera (1024x1024 pixels) with a 525/45 nm emission filter, an EM gain of 300, no binning, a 30 ms exposure time, and readout mode (EM Gain) set to 30 MHz at 16-bit. Excitation was achieved using a 488 nm solid-state laser at 5% of its maximum power (0.1 mW at the objective). This

setup allowed for a sufficient contrast while limiting phototoxicity. Images were acquired at 1-second intervals. Recordings lasted between 105 and 150 minutes to maximise Ca^{2+} spike detection per cell. Examples of recorded spike trains are shown in Fig 2.

Analysis of $[Ca^{2+}]_i$ spike trains

Time-lapse image series were analysed with Nikon's NIS-Elements AR software (version 5.21.03) [91], which was used to define regions of interest (ROIs) and extract fluorescence intensity measurements. ROIs were drawn following the contours of the cells and their shape was adjusted over time using the 'Edit ROIs in Time' tool to match cell rearrangements during acquisition. We performed baseline correction of the spike trains using the PeakUtils Python package [92] and then normalised the intensities to the average corrected baseline (F_0). Ca^{2+} spikes were detected and characterised using the PyCaSig software [93]. This GUI-based Python program automates the processing of $[Ca^{2+}]_i$ time series data and computes measures of spike properties. As previously described [9], only the stationary components of spike sequences were considered for ISI analysis.

In our experiments, HEK293 cells are subjected to prolonged CCh stimulation, which can cause receptor desensitisation and other slow processes that lead to changes in the average ISIs throughout the duration of a spike train [94,95]. Slow trends on the time scale of a few times the average ISI entail contributions, especially to higher moments and cumulants, which are not related to the stochastic aspects of spike generation. We applied two measures to avoid these contributions: if a spike train exhibits segments comprising several ISIs with different average ISIs, we analysed those segments separately as further explained in S1 Text, Sect D. Such segments are marked in Fig 2A, 2B and 2D. Furthermore, residual linear trends within these segments were removed before the calculation of the standard deviation and correlation coefficients. The removal of trends did not change the average (S1 Text, Sect D). Only stationary sequences of spike trains with at least 11 recorded spikes were included in the analysis of average ISI and with at least 15 spikes in the analysis of SD and correlations.

Supporting information

S1 Text. Section A. Calculating moments of the first passage time distribution. Section B. Numerical methods. Section C. Comments on the CICR-factor r_n. Section D. Comments on determining stationary ISI sequences.
(PDF)

Acknowledgments

We thank Matthias Richter and the other members of the Advanced Light Microscopy & Image Analysis platform of the Max Delbrück Center for Molecular Medicine for their support, help and advice.

Author contributions

Conceptualization: Martin Falcke.

Data curation: Caterina Azzoni, Martin Falcke.

Formal analysis: Caterina Azzoni, Martin Falcke.

Investigation: Caterina Azzoni, Martin Falcke.

Methodology: Caterina Azzoni, Anje Sporbert, H. Llewelyn Roderick, Martin Falcke.

Project administration: Caterina Azzoni, Michael Gotthardt, Martin Falcke.

Resources: H. Llewelyn Roderick, Anje Sporbert, Michael Gotthardt, Martin Falcke.

Software: Caterina Azzoni, Martin Falcke.

Supervision: Rene Jüttner, Anje Sporbert, Michael Gotthardt, H. Llewelyn Roderick, Martin Falcke.

Validation: Caterina Azzoni, H. Llewelyn Roderick, Martin Falcke.

Visualization: Caterina Azzoni, Martin Falcke.

Writing – original draft: Caterina Azzoni, Martin Falcke.

Writing – review & editing: Caterina Azzoni, Rene Jüttner, Anje Sporbert, Michael Gotthardt, H. Llewelyn Roderick, Martin Falcke.

References

1. Thul R, Falcke M. Release currents of $IP_{(3)}$ receptor channel clusters and concentration profiles. Biophys J. 2004;86(5):2660–73. https://doi.org/10.1016/S0006-3495(04)74322-2 PMID: 15111387
2. Bentele K, Falcke M. Quasi-steady approximation for ion channel currents. Biophys J. 2007;93(8):2597–608. https://doi.org/10.1529/biophysj.107.104299 PMID: 17586567
3. Vais H, Foskett JK, Mak D-OD. Unitary Ca(2+) current through recombinant type 3 InsP(3) receptor channels under physiological ionic conditions. J Gen Physiol. 2010;136(6):687–700. https://doi.org/10.1085/jgp.201010513 PMID: 21078871
4. Bezprozvanny I, Ehrlich BE. Inositol (1,4,5)-trisphosphate (InsP3)-gated Ca channels from cerebellum: conduction properties for divalent cations and regulation by intraluminal calcium. J Gen Physiol. 1994;104(5):821–56. https://doi.org/10.1085/jgp.104.5.821 PMID: 7876825
5. Rossi AM, Tovey SC, Rahman T, Prole DL, Taylor CW. Analysis of IP_3 receptors in and out of cells. Biochim Biophys Acta. 2012;1820(8):1214–27. https://doi.org/10.1016/j.bbagen.2011.10.004 PMID: 22033379
6. Berridge MJ, Bootman MD, Lipp P. Calcium–a life and death signal. Nature. 1998;395(6703):645–8. https://doi.org/10.1038/27094 PMID: 9790183
7. Taylor CW. Why do hormones stimulate Ca2 mobilization. Biochem Soc Trans. 1995;23:637–42. https://doi.org/10.1042/bst0230637 PMID: 8566433
8. Thul R, Bellamy TC, Roderick HL, Bootman MD, Coombes S. Calcium oscillations. In: Maroto M, Monk NAM, editors. Cellular oscillatory mechanisms. New York: Springer; 2009. p. 1–27. https://doi.org/10.1007/978-0-387-09794-7_1
9. Thurley K, Tovey SC, Moenke G, Prince VL, Meena A, Thomas AP. Reliable encoding of stimulus intensities within random sequences of intracellular Ca2 spikes. Sci Signal. 2014;7(331):ra59. https://doi.org/10.1126/scisignal.2005237
10. Dupont G, Combettes L, Bird GS, Putney JW. Calcium oscillations. Cold Spring Harbor Perspectives in Biology. 2011;3(3). https://doi.org/10.1101/cshperspect.a004226
11. Schipke CG, Heidemann A, Skupin A, Peters O, Falcke M, Kettenmann H. Temperature and nitric oxide control spontaneous calcium transients in astrocytes. Cell Calcium. 2008;43(3):285–95. https://doi.org/10.1016/j.ceca.2007.06.002 PMID: 17698190
12. Bootman M, Berridge M, Lipp P. Cooking with calcium: the recipes for composing global signals from elementary events. Cell. 1997;91:367–73. https://doi.org/10.1016/s0092-8674(00)80420-1
13. Skupin A, Kettenmann H, Winkler U, Wartenberg M, Sauer H, Tovey SC, et al. How does intracellular Ca^{2+} oscillate: by chance or by the clock?. Biophys J. 2008;94(6):2404–11. https://doi.org/10.1529/biophysj.107.119495 PMID: 18065468
14. Powell J, Falcke M, Skupin A, Bellamy TC, Kypraios T, Thul R. A statistical view on calcium oscillations. In: Islam MS, editor. Advances in experimental medicine and biology. Cham: Springer; 2020. p. 799–826. https://doi.org/10.1007/978-3-030-12457-1_32
15. Dragoni S, Laforenza U, Bonetti E, Lodola F, Bottino C, Berra-Romani R, et al. Vascular endothelial growth factor stimulates endothelial colony forming cells proliferation and tubulogenesis by inducing

oscillations in intracellular Ca^{2+} concentration. Stem Cells. 2011;29(11):1898–907. https://doi.org/10.1002/stem.734 PMID: 21905169

16. Oprea L, Desjardins N, Jiang X, Sareen K, Zheng JQ, Khadra A. Characterizing spontaneous Ca^{2+} local transients in OPCs using computational modeling. Biophysical Journal. 2022;121(23):4419–32. https://doi.org/10.1016/j.bpj.2022.11.007
17. Cao P, Tan X, Donovan G, Sanderson MJ, Sneyd J. A deterministic model predicts the properties of stochastic calcium oscillations in airway smooth muscle cells. PLoS Comput Biol. 2014;10(8):e1003783. https://doi.org/10.1371/journal.pcbi.1003783 PMID: 25121766
18. Keizer J, Smith GD, Ponce-Dawson S, Pearson JE. Saltatory propagation of Ca^{2+} waves by Ca^{2+} sparks. Biophys J. 1998;75(2):595–600. https://doi.org/10.1016/S0006-3495(98)77550-2 PMID: 9675162
19. Jung P, Shuai JW. Optimal sizes of ion channel clusters. Europhys Lett. 2001;56(1):29–35.
20. Falcke M. On the role of stochastic channel behavior in intracellular Ca^{2+} dynamics. Biophys J. 2003;84(1):42–56. https://doi.org/10.1016/S0006-3495(03)74831-0 PMID: 12524264
21. Sneyd J, Falcke M, Dufour J-F, Fox C. A comparison of three models of the inositol trisphosphate receptor. Prog Biophys Mol Biol. 2004;85(2–3):121–40. https://doi.org/10.1016/j.pbiomolbio.2004.01.013 PMID: 15142740
22. Jung P, Swaminathan D, Ullah A. Calcium spikes: chance or necessity?. Chemical Physics. 2010;375(2–3):625–9. https://doi.org/10.1016/j.chemphys.2010.05.010
23. Kummer U, Krajnc B, Pahle J, Green AK, Dixon CJ, Marhl M. Transition from stochastic to deterministic behavior in calcium oscillations. Biophys J. 2005;89(3):1603–11. https://doi.org/10.1529/biophysj.104.057216 PMID: 15994893
24. Calabrese A, Fraiman D, Zysman D, Ponce Dawson S. Stochastic fire-diffuse-fire model with realistic cluster dynamics. Phys Rev E Stat Nonlin Soft Matter Phys. 2010;82(3 Pt 1):031910. https://doi.org/10.1103/PhysRevE.82.031910 PMID: 21230111
25. Perc M, Green AK, Dixon CJ, Marhl M. Establishing the stochastic nature of intracellular calcium oscillations from experimental data. Biophys Chem. 2008;132(1):33–8. https://doi.org/10.1016/j.bpc.2007.10.002 PMID: 17964062
26. Dupont G, Abou-Lovergne A, Combettes L. Stochastic aspects of oscillatory Ca^{2+} dynamics in hepatocytes. Biophys J. 2008;95(5):2193–202. https://doi.org/10.1529/biophysj.108.133777 PMID: 18515398
27. Dupont G, Combettes L. What can we learn from the irregularity of Ca2 oscillations?. Chaos. 2009;19(3):037112. https://doi.org/10.1063/1.3160569
28. Wacquier B, Voorsluijs V, Combettes L, Dupont G. Coding and decoding of oscillatory Ca^{2+} signals. Semin Cell Dev Biol. 2019;94:11–9. https://doi.org/10.1016/j.semcdb.2019.01.008 PMID: 30659886
29. Cao P, Falcke M, Sneyd J. Mapping interpuff interval distribution to the properties of inositol trisphosphate receptors. Biophys J. 2017;112(10):2138–46. https://doi.org/10.1016/j.bpj.2017.03.019 PMID: 28538151
30. Cao P, Donovan G, Falcke M, Sneyd J. A stochastic model of calcium puffs based on single-channel data. Biophys J. 2013;105(5):1133–42. https://doi.org/10.1016/j.bpj.2013.07.034 PMID: 24010656
31. Ramlow L, Falcke M, Lindner B. An integrate-and-fire approach to Ca^{2+} signaling. Part I: Renewal model. Biophys J. 2023;122(4):713–36. https://doi.org/10.1016/j.bpj.2023.01.007 PMID: 36635961
32. Taylor CW, Thorn P. Calcium signalling: IP_3 rises again...and again. Curr Biol. 2001;11(9):R352-5. https://doi.org/10.1016/s0960-9822(01)00192-0 PMID: 11369246
33. Smith IF, Parker I. Imaging the quantal substructure of single IP_3R channel activity during Ca2 puffs in intact mammalian cells. Proc Nat Acad Sci USA. 2009;106(15):6404–9. https://doi.org/10.1073/pnas.0810799106
34. Wiltgen SM, Smith IF, Parker I. Superresolution localization of single functional IP_3R channels utilizing Ca2 flux as a readout. Biophysical Journal. 2010;99(2):437–46. https://doi.org/10.1016/j.bpj.2010.04.037
35. Dickinson GD, Swaminathan D, Parker I. The probability of triggering calcium puffs is linearly related to the number of inositol trisphosphate receptors in a cluster. Biophys J. 2012;102(8):1826–36. https://doi.org/10.1016/j.bpj.2012.03.029 PMID: 22768938
36. Lock JT, Alzayady KJ, Yule DI, Parker I. All three IP_3 receptor isoforms generate Ca^{2+} puffs that display similar characteristics. Sci Signal. 2018;11(561):eaau0344. https://doi.org/10.1126/scisignal.aau0344 PMID: 30563861
37. Lock JT, Parker I. IP_3 mediated global Ca^{2+} signals arise through two temporally and spatially distinct modes of Ca^{2+} release. Elife. 2020;9:e55008. https://doi.org/10.7554/eLife.55008 PMID: 32396066

38. Bootman M, Niggli E, Berridge M, Lipp P. Imaging the hierarchical Ca^{2+} signalling system in HeLa cells. J Physiol. 1997;499(Pt 2):307–14. https://doi.org/10.1113/jphysiol.1997.sp021928 PMID: 9080361
39. Smith IF, Wiltgen SM, Parker I. Localization of puff sites adjacent to the plasma membrane: functional and spatial characterization of Ca^{2+} signaling in SH-SY5Y cells utilizing membrane-permeant caged IP_3. Cell Calcium. 2009;45(1):65–76. https://doi.org/10.1016/j.ceca.2008.06.001 PMID: 18639334
40. Taufiq-Ur-Rahman, Skupin A, Falcke M, Taylor CW. Clustering of InsP3 receptors by InsP3 retunes their regulation by InsP3 and Ca^{2+}. Nature. 2009;458(7238):655–9. https://doi.org/10.1038/nature07763 PMID: 19348050
41. Suhara W, Kobayashi M, Sagara H, Hamada K, Goto T, Fujimoto I, et al. Visualization of inositol 1,4,5-trisphosphate receptor by atomic force microscopy. Neurosci Lett. 2006;391(3):102–7. https://doi.org/10.1016/j.neulet.2005.08.066 PMID: 16198054
42. Keebler MV, Taylor CW. Endogenous signalling pathways and caged IP_3 evoke Ca^{2+} puffs at the same abundant immobile intracellular sites. J Cell Sci. 2017;130(21):3728–39. https://doi.org/10.1242/jcs.208520 PMID: 28893841
43. Yao Y, Choi J, Parker I. Quantal puffs of intracellular Ca^{2+} evoked by inositol trisphosphate in Xenopus oocytes. J Physiol. 1995;482(Pt 3):533–53. https://doi.org/10.1113/jphysiol.1995.sp020538 PMID: 7738847
44. Marchant J, Callamaras N, Parker I. Initiation of $IP_{(3)}$-mediated Ca(2+) waves in Xenopus oocytes. EMBO J. 1999;18(19):5285–99. https://doi.org/10.1093/emboj/18.19.5285 PMID: 10508162
45. Skupin A, Kettenmann H, Falcke M. Calcium signals driven by single channel noise. PLoS Comput Biol. 2010;6(8):e1000870. https://doi.org/10.1371/journal.pcbi.1000870 PMID: 20700497
46. Marchant JS, Parker I. Role of elementary Ca(2+) puffs in generating repetitive Ca(2+) oscillations. EMBO J. 2001;20(1–2):65–76. https://doi.org/10.1093/emboj/20.1.65 PMID: 11226156
47. Vorontsova I, Lock JT, Parker I. KRAP is required for diffuse and punctate IP_3-mediated Ca^{2+} liberation and determines the number of functional IP_3R channels within clusters. Cell Calcium. 2022;107:102638. https://doi.org/10.1016/j.ceca.2022.102638 PMID: 36030740
48. Thillaiappan NB, Smith HA, Atakpa-Adaji P, Taylor CW. KRAP tethers IP_3 receptors to actin and licenses them to evoke cytosolic Ca^{2+} signals. Nat Commun. 2021;12(1):4514. https://doi.org/10.1038/s41467-021-24739-9 PMID: 34301929
49. Ivanova A, Atakpa-Adaji P, Rao S, Marti-Solano M, Taylor CW. Dual regulation of IP_3 receptors by IP_3 and PIP2 controls the transition from local to global Ca^{2+} signals. Mol Cell. 2024;84(20):3997-4015.e7. https://doi.org/10.1016/j.molcel.2024.09.009 PMID: 39366376
50. Croft W, Reusch K, Tilunaite A, Russell NA, Thul R, Bellamy TC. Probabilistic encoding of stimulus strength in astrocyte global calcium signals. Glia. 2016;64(4). https://doi.org/10.1002/glia.22947
51. Tilūnaitė A, Croft W, Russell N, Bellamy TC, Thul R. A Bayesian approach to modelling heterogeneous calcium responses in cell populations. PLoS Comput Biol. 2017;13(10):e1005794. https://doi.org/10.1371/journal.pcbi.1005794 PMID: 28985235
52. Gin E, Falcke M, Wagner LE 2nd, Yule DI, Sneyd J. A kinetic model of the inositol trisphosphate receptor based on single-channel data. Biophys J. 2009;96(10):4053–62. https://doi.org/10.1016/j.bpj.2008.12.3964 PMID: 19450477
53. Thurley K, Smith IF, Tovey SC, Taylor CW, Parker I, Falcke M. Timescales of $IP_{(3)}$-evoked Ca(2+) spikes emerge from Ca(2+) puffs only at the cellular level. Biophys J. 2011;101(11):2638–44. https://doi.org/10.1016/j.bpj.2011.10.030 PMID: 22261051
54. Berridge MJ, Lipp P, Bootman MD. The versatility and universality of calcium signalling. Nat Rev Mol Cell Biol. 2000;1(1):11–21. https://doi.org/10.1038/35036035 PMID: 11413485
55. Bird GSJ, Rossier MF, Obie JF, J W JP. Sinusoidal oscillations in intracellular calcium due to negative feedback by protein kinase C. J Biol Chem. 1993;268(12):8425–8.
56. Matsu-ura T, Michikawa T, Inoue T, Miyawaki A, Yoshida M, Mikoshiba K. Cytosolic inositol 1,4,5-trisphosphate dynamics during intracellular calcium oscillations in living cells. The Journal of Cell Biology. 2006;173(5):755–65. https://doi.org/10.1083/jcb.200512141 PMID: 16754959
57. Politi A, Gaspers LD, Thomas AP, Höfer T. Models of IP_3 and Ca^{2+} oscillations: frequency encoding and identification of underlying feedbacks. Biophys J. 2006;90(9):3120–33. https://doi.org/10.1529/biophysj.105.072249 PMID: 16500959
58. Bartlett PJ, Metzger W, Gaspers LD, Thomas AP. Differential regulation of multiple steps in inositol 1,4,5-trisphosphate signaling by protein kinase C shapes hormone-stimulated Ca2 oscillations. J Biol Chem. 2015;290(30):18519–33. https://doi.org/10.1074/jbc.M115.657767 PMID: 26078455
59. Strassheim D, Williams CL. P2Y2 purinergic and M3 muscarinic acetylcholine receptors activate different phospholipase C-beta isoforms that are uniquely susceptible to protein kinase

C-dependent phosphorylation and inactivation. J Biol Chem. 2000;275(50):39767–72. https://doi.org/10.1074/jbc.M007775200 PMID: 10995776

60. Ishii M, Kurachi Y. Muscarinic acetylcholine receptors. Current Pharmaceutical Design. 2006;12(28):3573–81. https://doi.org/10.2174/138161206778522056
61. Cooper RH, Coll KE, Williamson JR. Differential effects of phorbol ester on phenylephrine and vasopressin-induced Ca^{2+} mobilization in isolated hepatocytes.. Journal of Biological Chemistry. 1985;260(6):3281–8. https://doi.org/10.1016/s0021-9258(19)83618-9
62. Rooney TA, Sass EJ, Thomas AP. Characterization of cytosolic calcium oscillations induced by phenylephrine and vasopressin in single fura-2-loaded hepatocytes. J Biol Chem. 1989;264(29):17131–41. PMID: 2793847
63. Dixon C, Cobbold P, Green A. Oscillations in cytosolic free Ca2 induced by ADP and ATP in single rat hepatocytes display differential sensitivity to application of phorbol ester. Biochem J. 1995;309:145–9. https://doi.org/10.1042/bj3090145
64. Lipp P, Reither G. Protein kinase C: the "masters" of calcium and lipid. Cold Spring Harb Perspect Biol. 2011;3(7):a004556. https://doi.org/10.1101/cshperspect.a004556 PMID: 21628429
65. Corrêa-Velloso JC, Bartlett PJ, Brumer R, Gaspers LD, Ulrich H, Thomas AP. Receptor-specific Ca2 oscillation patterns mediated by differential regulation of P2Y purinergic receptors in rat hepatocytes. iScience. 2021;24(10):103139. https://doi.org/10.1016/j.isci.2021.103139
66. Falcke M, Friedhoff VN. The stretch to stray on time: resonant length of random walks in a transient. Chaos. 2018;28(5):053117. https://doi.org/10.1063/1.5023164 PMID: 29857685
67. Friedhoff VN, Lindner B, Falcke M. Modeling IP_3-induced Ca^{2+} signaling based on its interspike interval statistics. Biophys J. 2023;122(13):2818–31. https://doi.org/10.1016/j.bpj.2023.06.004 PMID: 37312455
68. Bezprozvanny I, Watras J, Ehrlich BE. Bell-shaped calcium-response curves of Ins(1,4,5)P3- and calcium-gated channels from endoplasmic reticulum of cerebellum. Nature. 1991;351(6329):751–4. https://doi.org/10.1038/351751a0 PMID: 1648178
69. De Young GW, Keizer J. A single-pool inositol 1,4,5-trisphosphate-receptor-based model for agonist-stimulated oscillations in Ca^{2+} concentration. Proc Natl Acad Sci U S A. 1992;89(20):9895–9. https://doi.org/10.1073/pnas.89.20.9895 PMID: 1329108
70. Marchant JS, Taylor CW. Cooperative activation of IP_3 receptors by sequential binding of IP_3 and Ca^{2+} safeguards against spontaneous activity. Curr Biol. 1997;7(7):510–8. https://doi.org/10.1016/s0960-9822(06)00222-3 PMID: 9210378
71. Foskett JK, White C, Cheung K-H, Mak D-OD. Inositol trisphosphate receptor Ca^{2+} release channels. Physiol Rev. 2007;87(2):593–658. https://doi.org/10.1152/physrev.00035.2006 PMID: 17429043
72. Siekmann I, Wagner LE 2nd, Yule D, Crampin EJ, Sneyd J. A kinetic model for type I and II IP_3R accounting for mode changes. Biophys J. 2012;103(4):658–68. https://doi.org/10.1016/j.bpj.2012.07.016 PMID: 22947927
73. Dupont G, Falcke M, Kirk V, Sneyd J. Models of calcium signalling. In: Antman SS, Greengard L, Holmes PJ, editors. Interdisciplinary applied mathematics. Springer; 2016. https://doi.org/10.1007/978-3-319-29647-0
74. van Kampen NG. Stochastic processes in physics and chemistry. Amsterdam: North-Holland. 2001.
75. Hernandez E, Leite MF, Guerra MT, Kruglov EA, Bruna-Romero O, Rodrigues MA, et al. The spatial distribution of inositol 1,4,5-trisphosphate receptor isoforms shapes Ca^{2+} waves. J Biol Chem. 2007;282(13):10057–67. https://doi.org/10.1074/jbc.M700746200 PMID: 17284437
76. Hillson EJ, Hallett MB. Localised and rapid Ca^{2+} micro-events in human neutrophils: conventional Ca^{2+} puffs and global waves without peripheral-restriction or wave cycling. Cell Calcium. 2007;41(6):525–36. https://doi.org/10.1016/j.ceca.2006.10.010 PMID: 17324458
77. Dupont G, Swillens S, Clair C, Tordjmann T, Combettes L. Hierarchical organization of calcium signals in hepatocytes: from experiments to models. Biochim Biophys Acta. 2000;1498(2–3):134–52. https://doi.org/10.1016/s0167-4889(00)00090-2 PMID: 11108957
78. Bartlett PJ, Cloete I, Sneyd J, Thomas AP. IP_3-Dependent Ca^{2+} oscillations switch into a dual oscillator mechanism in the presence of PLC-linked hormones. iScience. 2020;23(5):101062. https://doi.org/10.1016/j.isci.2020.101062 PMID: 32353764
79. Sherman A, Smith GD, Dai L, Miura RM. Asymptotic analysis of buffered calcium diffusion near a point source. SIAM J Appl Math. 2001;61(5):1816–38. https://doi.org/10.1137/s0036139900368996
80. Schendel T, Falcke M. Efficient and detailed model of the local Ca^{2+} release unit in the ventricular cardiac myocyte. Genome Inform. 2010;22:142–55. PMID: 20238425

81. Vais H, Wang M, Mallilankaraman K, Payne R, McKennan C, Lock JT, et al. ER-luminal [Ca^{2+}] regulation of InsP3 receptor gating mediated by an ER-luminal peripheral Ca^{2+}-binding protein. Elife. 2020;9:e53531. https://doi.org/10.7554/eLife.53531 PMID: 32420875
82. Bootman MD, Missiaen L, Parys JB, Smedt HD, Casteels R. Control of inositol 1,4,5-trisphosphate-induced Ca2 release by cytosolic Ca2. Biochem J. 1995;306(2):445–51. https://doi.org/10.1042/bj3060445
83. Bezprozvanny I, Ehrlich BE. ATP modulates the function of inositol 1,4,5-trisphosphate-gated channels at two sites. Neuron. 1993;10(6):1175–84. https://doi.org/10.1016/0896-6273(93)90065-y PMID: 7686381
84. Mak DD, McBride S, Foskett JK. ATP regulation of type 3 inositol 1,4,5-trisphosphate receptor channel gating by allosteric tuning of Ca^{2+} activation. J Gen Physiol. 2001;117:447–56. https://doi.org/10.1085/jgp.117.5.447
85. Betzenhauser MJ, Wagner LE 2nd, Iwai M, Michikawa T, Mikoshiba K, Yule DI. ATP modulation of Ca^{2+} release by type-2 and type-3 inositol (1, 4, 5)-triphosphate receptors. Differing ATP sensitivities and molecular determinants of action. J Biol Chem. 2008;283(31):21579–87. https://doi.org/10.1074/jbc.M801680200 PMID: 18505727
86. Thurley K, Skupin A, Thul R, Falcke M. Fundamental properties of Ca^{2+} signals. Biochim Biophys Acta. 2012;1820(8):1185–94. https://doi.org/10.1016/j.bbagen.2011.10.007 PMID: 22040723
87. Skupin A, Falcke M. Statistical properties and information content of calcium oscillations. Genome Inform. 2007;18:44–53. PMID: 18546473
88. Skupin A, Falcke M. Statistical analysis of calcium oscillations. Eur Phys J Spec Top. 2010;187(1):231–40. https://doi.org/10.1140/epjst/e2010-01288-9
89. Givré A, Ponce Dawson S. Information content in stochastic pulse sequences of intracellular messengers. Front Phys. 2018;6. https://doi.org/10.3389/fphy.2018.00074
90. Thurley K, Falcke M. Derivation of Ca^{2+} signals from puff properties reveals that pathway function is robust against cell variability but sensitive for control. Proc Natl Acad Sci U S A. 2011;108(1):427–32. https://doi.org/10.1073/pnas.1008435108 PMID: 21173273
91. Nikon C. NIS-Elements AR Analysis Software, Version 5.21.03; 2021. [cited 2024 Nov 9]. https://www.microscope.healthcare.nikon.com/products/software/nis-elements
92. Negri LH, Vestri C. Lucashn/ peakutils: v1.1.0. Zenodo. 2017. https://doi.org/10.5281/zenodo.887917
93. Friedhoff VN. PyCaSig. 2024. [cited 2025 Jan 13]. https://github.com/nicouh/PyCaSig
94. Mundell SJ, Benovic JL. Selective regulation of endogenous G protein-coupled receptors by arrestins in HEK293 cells. J Biol Chem. 2000;275(17):12900–8. https://doi.org/10.1074/jbc.275.17.12900 PMID: 10777589
95. Stope MB, Kunkel C, Kories C, Schmidt M, Michel MC. Differential agonist-induced regulation of human M2 and M3 muscarinic receptors. Biochem Pharmacol. 2003;66(11):2099–105. https://doi.org/10.1016/s0006-2952(03)00580-x PMID: 14609734